Radiology: Imaging Cancer

Endogenous chemical exchange saturation transfer (CEST) MR imaging for the diagnosis and therapy response assessment of brain tumors: A systematic review

Journal:	*Radiology: Imaging Cancer*
Manuscript ID	RYCAN-19-0036.R1
Manuscript Type:	Original Research
Manuscript Categorization Terms:	MR-Imaging < 2. MODALITIES/TECHNIQUES, Neuro-Oncology < 2. MODALITIES/TECHNIQUES, Brain/Brain Stem < 5. STRUCTURES

SCHOLARONE™
Manuscripts

Endogenous chemical exchange saturation transfer (CEST) MR imaging for the

diagnosis and therapy response assessment of brain tumors: A systematic review

Sachi Okuchi, MD, PhD[1,2], Ahmed Hammam, MD[1], Xavier Golay, PhD[1], Mina Kim, PhD[1],

Stefanie Thust, MD, FRCR[1, 3]

1 Department of Brain Repair and Rehabilitation, University College London, Institute of

Neurology, Queen Square, London WC1N 3BG, UK.

2 Department of Diagnostic Imaging and Nuclear Medicine, Graduate School of Medicine,

Kyoto University, 54 Shogoin-Kawaharacho, Sakyo-ku, Kyoto 606-8507, Japan

3 Lysholm Department of Neuroradiology, National Hospital for Neurology and

Neurosurgery, Queen Square, London WC1N 3BG, UK.

Corresponding author: Sachi Okuchi, MD, PhD

Department of Diagnostic Imaging and Nuclear Medicine

Graduate School of Medicine, Kyoto University

54 Shogoin-Kawaharacho, Sakyo-ku, Kyoto 606-8507, Japan

Tel: +81-75-751-3760

Email: sachi.okuchi@gmail.com

Manuscript type: Original Research (systematic review)

Word Count for Text: 5147 words (Introduction to Discussion)

Endogenous chemical exchange saturation transfer (CEST) MR imaging for the diagnosis and therapy response assessment of brain tumors: A systematic review

Article type: Original Research

Key Points

• Endogenous CEST methods can support glioma grading, molecular subtyping and differential diagnosis.

• CEST signal may aid the identification of metabolically active tumor following treatment.

• Study data are heterogeneous with a substantial bias risk, highlighting the importance of future prospective research and technical standardization.

Summary statement

CEST can act as a biomarker for metabolically active brain tumors, evidenced by correlations to tissue findings including proliferative indices. But further study is required to assess its diagnostic power with respect to specific clinical indications.

Conflict of interest

None declared.

1
2
3
4
5
6
7
8
9
10
11
12
13
14
15
16
17
18
19
20
21
22
23
24
25
26
27
28
29
30
31
32
33
34
35
36
37
38
39
40
41
42
43
44
45
46
47
48
49
50
51
52
53
54
55
56
57
58
59
60

Abbreviations

APT	Amide proton transfer
AUC	Area under the curve
CEST	Chemical exchange saturation transfer
Cho	Choline
Cr	Creatine
DSC	Dynamic susceptibility contrast-enhanced MRI
dns	downfield-rNOE-suppressed
FDG-PET	^{18}F-Fluorodeoxyglucose positron emission tomography
GBM	Glioblastoma
HGG	High grade glioma
IDH	Isocitrate dehydrogenase
LGG	Low grade glioma
MET	11C Methionine
MGMT	Methylguanyl methyltransferase
MTR$_{asym}$	Magnetisation transfer ratio asymmetry
NAA	N-acetylaspartate
NAWM	Normal appearing white matter
NOE	Nuclear Overhauser Enhancement
PRISMA-DTA	Preferred Reporting Items for Systematic Reviews and Meta-Analysis of Diagnostic Test Accuracy Studies
rCBV	Relative cerebral blood volume
RF	Radiofrequency
ROC	Receiver operating characteristic
ROI	Region of interest
SBM	Solitary brain metastasis/metastases
WHO	World Health Organization

Abstract

Purpose: To generate a narrative synthesis of published data on the use of endogenous chemical exchange saturation transfer (CEST) MR imaging in brain tumors.

Materials and Methods: A systematic database search (PubMed, Ovid Embase, Cochrane Library) was used to collate eligible studies. Two researchers independently screened publications according to predefined exclusion and inclusion criteria, followed by comprehensive data extraction. All included studies were subjected to a bias risk assessment using the Quality Assessment of Diagnostic Accuracy Studies (QUADAS-2) tool.

Results: The electronic database search identified 430 studies, of which 36 studies fulfilled the inclusion criteria. The final selection of included studies was categorized into 5 groups as follows: grading gliomas, 19 studies (areas under the curve (AUC) 0.500-1.000); predicting molecular subtypes of gliomas, 5 studies (AUC 0.610-0.920); distinction of different brain tumor types, 7 studies (AUC 0.707-0.905); therapy response assessment, 3 studies (AUC not given) and differentiating recurrence from treatment-related changes, 5 studies (AUC 0.880-0.980). A high bias risk was observed in a substantial proportion of studies.

Conclusion: Endogenous CEST imaging offers valuable, potentially unique information in brain tumors, but its diagnostic accuracy remains incompletely known. Further research is required to assess the method's role in support of molecular genetic diagnosis, to investigate its use in the post treatment phase, and to compare techniques with a view to standardization.

Introduction

Gliomas account for the majority of malignant intrinsic brain tumors in adults and despite being a relatively rare disease represent a major cause of mortality (1). Diffuse gliomas are categorized into World Health Organization (WHO) grades II to IV, based on histological evidence of proliferation and vascular invasion. However, histological (World Health Organization, WHO) grade and glioma cell lineage (oligodendroglioma versus astrocytoma) are limited predictors of disease progression, which is predominantly influenced by genetic factors (2). Recent studies have identified molecular markers such as the isocitrate dehydrogenase (IDH) gene and methylguanyl methyltransferase (MGMT) enzyme as key determinants of clinical outcomes (1). The optimal treatment and overall prognosis of glioma subtypes depend on the combination of molecular features and histological grade (1), however tumor malignant potential remains incompletely captured by clinical imaging techniques (3). In addition, MR imaging features can overlap between gliomas and different brain tumors (e.g. lymphoma, metastases) to such extent that only tissue diagnosis is conclusive (3). In the postoperative phase, the combination of radiation and chemotherapy with temozolomide may result in predominantly transient (pseudoprogression) or permanent (radiation necrosis) phenomena, which notoriously resemble contrast enhancing tumor progression due to blood-brain-barrier breakdown. A definitive distinction of these entities frequently requires serial imaging using a combination of structural and advanced techniques (4).

Chemical exchange saturation transfer (CEST) represents a promising novel imaging technique that has recently emerged as an alternative contrast mechanism for MRI (5). CEST signal can be generated through application of a radiofrequency (RF) 'saturation' pulse targeted at the resonance frequency of solute (e.g protein or metabolite bound) protons, from which the saturation is transferred to bulk water via chemical exchange. The much larger

water proton pool ensures a continuous flux of unsaturated protons close to the exchangeable

sites, thereby leading to a measurable reduction in the water signal amplitude after a few

seconds (6). CEST contrasts are classified into diamagnetic CEST, mostly consisting of

endogenous agents and paramagnetic CEST, which usually involves the use of exogenous

agent administration (6). Diamagnetic CEST utilizes chemical compounds with a range

between 0-7 ppm from water (-NH, -NH2, -OH groups etc.), representing the first discovered

and most studied CEST contrast (7). CEST techniques can be classified based on the type of

molecular construct, such as amide proton transfer (APT), amineCEST, glucoCEST (glucose-

based CEST contrast), gagCEST (CEST contrast originating from glycosaminoglycans), etc

(6). APT imaging targets endogenous mobile proteins and peptides featuring amide protons

and is the most widely used CEST imaging method, whereby the APT-weighted signal can be

quantified by magnetisation transfer ratio asymmetry (MTR_{asym}) analysis at +3.5 ppm, using

the water peak as reference (5). In addition, nuclear Overhauser enhancement (NOE)

mediated signal arises from mobile protein and lipid spin cross-relaxation effects between 0

and -5 ppm (8). It has been proposed that NOE could also become an imaging biomarker to

characterize brain tumors, similar to APT (9). Numerous single center studies have

highlighted the potential of CEST-MRI in stratifying brain tumors, however, the exact

diagnostic contribution of the method remains uncertain. To date, a single systematic review

and meta-analysis evaluated the diagnostic performance of only APT in grading gliomas (10).

To our knowledge, this is the first systematic review to explore the diagnostic and prognostic

value of endogenous CEST for a variety of brain tumor indications. Our analysis aims to

evaluate (a) the diagnostic value for grading gliomas, (b) the accuracy for predicting glioma

molecular subtypes, (c) the distinction of glioma from other brain tumor types, (d) the

assessment of brain tumors therapy response and (e) the power of differentiating tumor

recurrence from treatment-related changes.

Materials and Methods

This study was performed according to the Preferred Reporting Items for Systematic Reviews and Meta-Analysis of Diagnostic Test Accuracy Studies (PRISMA-DTA) criteria (11). The research was registered in the PROSPERO online database of systematic reviews (CRD42019122320).

Search strategy

A systematic search was performed in November 2018 by a medical researcher in PubMed, Ovid Embase and the Cochrane Library. We used the following search key words: ("brain tumor", "glioma", "brain neoplasm", "brain metastasis", "glioblastoma") and ("CEST", "chemical exchange saturation transfer", "amide proton transfer", "magnetization transfer", "chemical exchange", "nuclear Overhauser effect"). Further details of the search strategy are shown in **Supplementary material 1**.

Selection criteria

The abstracts of all articles retrieved in the initial search were screened by two board-certified radiologists with research experience in neuro-oncology. Selected full text manuscripts were reviewed in detail to determine their relevance. A stepwise selection was performed by two independent reviewers according to the following criteria: The exclusion criteria were: (a) no CEST technique (e.g. CEST, APT, NOE) was performed; (b) no brain tumor patients were examined; (c) animal/laboratory study; (d) technical study or diagnostic/prognostic value in brain tumors not evaluated; (e) comparisons confined to different MRI acquisition technique; (f) review articles, case reports (defined as less than 5 cases), letters, commentaries, or conference proceedings; (g) non-English full-texts. The inclusion criteria were: (a) CEST technique performed on brain tumor patients prior, during or after treatment; (b) study

assessed diagnostic or prognostic value of CEST parameters in brain tumors, or examined

pseudoprogression or recurrent tumors. In cases of disagreement, this was resolved in

consensus with a senior reviewer.

Data extraction

Data from the included studies were documented with the use of a data extraction form to

derive the CEST parameter value(s), diagnostic or prognostic accuracy, and method

characteristics. The latter included study design, country of origin, number of patients,

participant age, tumor histology and, where available, molecular data, MRI field strength,

type of CEST contrast, CEST acquisition parameters, methods of correcting B0 field

inhomogeneity and region of interest (ROI) placements. The same two reviewers

independently performed the full-text screening followed by the data extraction, and any

discrepancies were resolved in consensus with the third reviewer.

Study Quality Assessment

The study quality was examined using the Quality Assessment of Diagnostic Accuracy

Studies (QUADAS-2) instrument (12). We evaluated concerns regarding applicability in 3

domains and the risk of bias in 4 different domains. Each study was independently assessed

for quality and potential bias by the same two researchers. Disagreements were resolved as

described above.

Statistical Analysis

Descriptive data are presented in form of a narrative synthesis, because of the perceived

heterogeneity of research questions, CEST technical parameters and brain tumor cohorts

studied.

Results

Search results

A total of 430 studies were identified using the electronic database searches. After removing duplicate studies and screening the studies titles and abstracts, 68 studies remained, which provisionally satisfied the inclusion criteria. Of these, 36 studies proved to be relevant in subsequent full-text screening. We categorized the final selection of 36 studies into 5 groups as follows: grading gliomas, 19 studies (9, 13-30); predicting molecular subtypes of gliomas, 5 studies (13, 14, 31-33); distinction of different brain tumor types, 7 studies (5, 8, 34-38); therapy response assessment, 3 studies (39-41) and differentiating recurrence from treatment-related changes, 5 studies (25, 42-45). Two studies (13, 14) contained data on glioma grading and predicting molecular subtypes, and one study (25) was assigned to both glioma grading and differentiating recurrence from treatment-related changes. A flowchart of the study selection process is presented in **Figure 1**. A summary of all studies included in the analysis is shown in **Table 1-6 (see supplement)**.

CEST techniques

Thirty-three studies of the searched 36 studies used APT weighted imaging. 6 studies presented NOE weighted images, and 4 studies trialed amine CEST. Three studies tested conventional MT imaging, which detect semi-solid macromolecules in the more solid environment of the cell than APT (37), and 1 study used fitted MT and NOE.

Glioma grading

A total of 596 glioma patients (1 WHO I, 232 WHO II, 129 WHO III, 193 WHO V, 41 WHO III-IV were included from 19 studies. Studies summarized WHO I and II into low grade gliomas (LGGs), whereby WHO I corresponds to indolent entities other than diffuse glioma,

e.g. pilocytic astrocytoma (2) and WHO III and IV into high grade glioma (HGGs).

Seventeen of 19 studies for glioma grading used light microscopic analysis according to the

WHO 2007 Classification of CNS Tumors; on the contrary only 2/19 (more recent) studies

adopted the WHO 2016 Classification of CNS Tumors as the diagnostic gold standard. Of

these, both studies performed immunohistochemistry testing for IDH1, and one study

performed analysis for MGMT genetic status. 5/19 studies reported the Ki-67 labeling index

as a biomarker of tumor cellularity. 17 studies used APT weighted imaging, 2 studies trialed

amine CEST, 2 studies presented NOE weighted images, and 1 study used fitted MT and

NOE. 17 studies used 3T MRI and 2 studies used 7T MRI. The imaging parameters and

grading results are shown in **Table 1** and **Table 2 (see supplement)**.

Statistically significant differences of APT signals between HGGs and LGGs (with

greater and lower signal, respectively) were identified in 16 of 17 studies using APT

weighted images ($p < 0.0001$-0.0497), aside from 1 study by Heo et al. which reported no

difference (9). Furthermore, significant differences were demonstrated between WHO grades

II, III and IV in studies Bai et al. (23) and Togao et al. (28), respectively. A significant

difference between WHO II and III but no difference between WHO III and IV was reported

in the studies by Zou et al. (15) and Jiang et al. (21). On the contrary, no difference was

shown between WHO II and III, but WHO III differed significantly from WHO IV in the

studies published by Choi et al. (22) and Sakata et al. (27). Receiver operating characteristic

(ROC) curve analyses were carried out in 13 of 17 studies. These demonstrated low to high

diagnostic performance with areas under the curve (AUC) of 0.500-1.000.

Paech et al. and Heo et al. evaluated NOE weighted MR images using 7T. Paech et al.

(13) showed a lower diagnostic performance for NOE weighted images than APT weighted

images and downfield-rNOE-suppressed (dns) APT. Conversely, Heo et al. (9) reported

NOE-based signals of HGGs were significantly lower than those of LGGs (P<0.05) without a statistical difference in APT-based signals.

Harris et al. performed 2 studies for evaluating diagnostic performance of gliomas using pH-weighted amine CEST (14, 26). The initial research in 2016 (26) yielded a statistically significant amine CEST signal difference for WHO glioma grades II, III and IV (P < 0.05 for WHO III versus IV and WHO II versus IV), but the subsequent study in 2018 (14) identified a difference only for WHO II versus WHO IV (P < 0.05). CEST signals increased with increasing tumor grades in both studies.

Some studies proposed a combination of CEST and multimodal techniques to increase the diagnostic accuracy. Zou et al. (15) reported that the combined use of intravoxel incoherent motion (IVIM) resulted in the increase of AUC from 0.957 to 0.986, Sakata et al. (17) observed that the combined use of FDG-PET improved the AUC from 0.76 to 0.85, and in a study by Choi et al. (22) the addition of relative cerebral blood volume (rCBV) derived from dynamic susceptibility contrast enhanced MRI (DSC) produced an AUC increase from 0.877 to 0.923. The correlation of APT signals and MRS parameters (choline (Cho), choline/N-acetylaspartate (NAA), NAA, Cho/creatine (Cr), NAA/Cr were investigated in 3 studies with moderate correlations (r=0.4-0.6).

Predicting molecular subtypes of gliomas

A total of 165 glioma patients (60 IDH^{wt}, 44 IDH^{mut}, 23 MGMT methylated, 17 MGMT unmethylated, 38 positive MGMT immunostaining, 4 negative MGMT immunostaining) were included from 5 studies. Three of 5 studies performed immunohistochemistry testing for IDH1, 2/5 studies performed for MGMT promotor methylation status, and 1/5 study performed for MGMT protein expression. The MGMT methylation status was assessed with a methylation-specific polymerase chain reaction and MGMT protein expression in tumor

cells was reviewed under a light microscopy. Four studies used APT-weighted imaging, 1 study performed amine CEST, 1 study used NOE weighted imaging and 1 study tested conventional MT imaging. Four studies were undertaken using 3T and 1 study using 7T magnetic field strength. Details of MR imaging parameters and molecular subtyping results are shown in **Table 1** and **Table 3 (see supplement)**.

Jiang et al (33) and Paech et al (13) investigated the value of CEST to predict IDH mutation status. Jiang et al reported a diagnostic accuracy of AUC 0.89 using a maximum ROI value ('hot spot') analysis of APT imaging in WHO II gliomas (n=27), with greater APT signal identified in IDH^{wt} gliomas. Paech et al proposed that dns APT had a high diagnostic performance (AUC 0.92-0.98) for IDH typing in a mixture of glioma WHO grades (II-IV, n=31) with increased APT signal in IDH^{wt} gliomas. Harris et al. (14) evaluated IDH status using pH-sensitive and oxygen-sensitive amine CEST, reporting marginally greater signal in IDH^{mut} (P = 0.0434).

Studies by Su et al. (31), Jiang et al. (2018) (32) and Paech et al (13) evaluated APT for the prediction of MGMT methylation status. Su et al reported a moderate diagnostic accuracy (AUC 0.849) for a visual scale (qualitative) assessment of APT characteristics. Tumors with greater signal intensity on the solid part or peripheral abnormality tended to be MGMT-positive gliomas. Jiang et al. observed a moderate performance (AUC 0.856) using histogram analysis of MTR_{asym} at 3.5ppm in comparison of the MGMT unmethylated glioblastomas (GBMs) versus the MGMT methylated GBMs. APT signals were significantly higher in the unmethylated GBMs than in the methylated GBMs (mean APT, P=0.022; $90\%_{tile}$ APT, P=0.006). Paech et al. presented APT and NOE results, which achieved low diagnostic accuracy (AUC 0.61-0.69) though slightly greater compared to perfusion (rCBV AUC 0.59) and diffusion-weighted MRI (apparent diffusion coefficient (ADC) AUC 0.59).

APT and NOE between the unmethylated gliomas than in the methylated gliomas had no statistically differences (P=0.13-0.39).

Distinction of different brain tumor types

A total of 215 patients (124 gliomas (4 WHO I, 20 WHO II, 17 WHO III, 77 WHO IV, 6 unclear), 59 metastases, 11 primary central nervous system lymphoma (PCNSL), 8 meningioma, 2 pituitary adenoma, 3 hemangioblastoma, 1 angiosarcoma, 6 cavernous malformation, 1 angiosarcoma) were included from 7 studies. Six brain metastases and non-tumor lesions were confirmed by clinical diagnosis, and the remaining tumors were confirmed by histopathology. The MR imaging parameters and CEST characteristics are shown in **Table 1** and **Table 4 (see supplement)**.

Yu et al (34) proposed that APT may have the ability to differentiate solitary brain metastases (SBM) from GBM. In their study of 45 SBM patients versus 43 GBM patients, APT values in perilesional tissue were significantly lower in the SBM group, whereby the $APTw_{min}$ values produced the highest AUC 0.905 compared to $APTw_{mean}$ values (AUC 0.868) for lesion discrimination.

Jiang et al (37) reported a high accuracy (AUC 0.963) for a subtraction parameter ($APTw_{max-min}$) to differentiate 11 PCNSLs from 21 HGGs, whereby the PCNSLs had significantly lower $APTw_{max-min}$ (0.76%±0.42%) than the HGGs (2.55%±1.20%). Jeong et al (36) compared APT signals in hemorrhagic brain lesions of 16 tumors and 7 non-neoplastic etiologies, observing that MTR_{asym} in acute to subacute hemorrhage was greater than in surrounding brain, regardless of the underlying pathology.

Park et al (38) analysed 45 Gadolinium-enhanced tumors, consisting of 19 'low grade' tumors (4 pilocytic astrocytoma, 2 hemangioblastoma, 3 low-grade astrocytoma, 7 low-grade oligodendroglioma, 3 pleomorphic xanthoastrocytoma) and 26 'high grade' tumors

(5 anaplastic astrocytomas, 3 anaplastic oligodendrogliomas, 2 anaplastic oligoastrocytomas, 11 GBM, 5 brain metastasis), reporting that APT $90\%_{tile}$ had AUC 0.85-0.86 in discriminating low grade tumor and high grade tumors. Compared with normalized $90\%_{tile}$ CBV (nCBV90) alone, adding APT90 significantly improved the AUC for the identification of contrast-enhanced low-grade tumor from 0.80-0.82 to 0.97.

Of 3 studies (5, 8, 35) featuring gliomas and meningiomas, Jones et al were the first group to demonstrate that the APT effect is quantifiable (8 gliomas and 2 meningiomas). Shen et al employed NOE maps, observing a significantly lower signal within tumor than contralateral normal appearing white matter for 6 gliomas (p<0.001) versus no significant difference for 5 meningiomas (P=0.116). Khlebnikov et al. used the effect of water T1 relaxation on APT to compare 3 different metrics of APT contrast: magnetization transfer ratio (MTR_{Rex}), relaxation-compensated MTR_{Rex} (AREX), and traditional asymmetry (MTR_{asym}) in 5 gliomas and 1 meningioma. This study identified a difference were appeared between LGG and HGG in non-Gadolinium-enhanced solid tumor regions using MTR_{Rex} and no difference in AREX.

Differentiating tumor recurrence from treatment-related changes

A total of 161 glioma patients (15 WHO II, 15 WHO III, 131 WHO IV; 108 tumor progression, 53 treatment related effects) and 16 brain metastasis patients (5 tumor progression, 11 radiation necrosis) were included from 5 studies. Final diagnoses were confirmed by second look surgery or clinic-radiologic follow up using the Response Assessment in Neuro-Oncology criteria. All studies used APT weighted imaging, and 1 study in addition assessed MT and NOE signals. All studies were completed on 3T MRI. The patient characteristics and study results are listed in **Table 1** and **Table 5 (see supplement)**.

One study (43) reported a significant difference between tumor progression and radiation necrosis for brain metastases. A ROC analysis was not performed, however NOE MTR and Amide MTR differed between tumor progression and radiation necrosis ($P<0.0001$). The remaining 4 studies (25, 42, 44, 45) enrolled glioma patients (15 WHO II, 15 WHO III, 131 WHO IV). In all 4 studies, APT signals were significantly higher in tumor progression than in therapy induced lesion changes with high diagnostic accuracies reported (AUC 0.88-0.98). Park et al. (2018) (42) compared APT and positron emission tomography (PET) imaging, reported greater diagnostic accuracy for APT than 11C methionine (MET)-PET. Previously, Park et al. (2016) (44) had combined Gadolinium enhancement features and normalized cerebral blood volume (nCBV) with APT, resulting in increased diagnostic accuracy (AUC 0.970 over APT alone (AUC 0.89) for the distinction of glioma recurrence from therapy effects.

Therapy response assessment and prognosis prediction

Three studies examined therapy response assessment and prognosis prediction using CEST MRI. Of note, each differs in their research purposes and investigated different types of brain tumors. The patient characteristics and study results are presented in **Table 1 and Table 6 (see supplement)**. Regnery et al. (39) examined NOE and APT signals in 20 GBM patients to predict early tumor progression after first-line treatment on 7T MRI. Pretreatment tumor signal in NOE - Lorentzian difference (LD) differed significantly based on responsiveness to first-line treatment (AUC=0.98).

Desmond et al. (40) evaluated the predictive value of various CEST metrics in 25 brain metastases treated with stereotactic radiosurgery (SRS) at baseline compared to 1 week post-treatment, and related these to changes in tumor volume at 1 month. A significant

association was observed between metastasis volume changes and the relative change in NOE

peak amplitude in contralateral NAWM.

Harris et al. (41) performed pH-weighted imaging in 20 GBM patients and evaluated

differences between acidic tumors and non-acidic tumors in progression free survival (PFS).

The median PFS intervals for acidic tumors and non-acidic tumors were 125 days and 450

days, respectively.

Study quality

The results of the study quality assessment using the QUADAS-2 tool are demonstrated in

Figure 2. Several studies had a high risk of bias regarding the selection of patients (17/36),

and/or concerning the conduct or interpretation of the index test (6/36) due to retrospective

design and/or ROI placement by a single researcher. In a high proportion of studies

(approximately 80%) it was unclear whether radiologists were blinded to histological results

when placing ROIs, and in approximately 50% it was unknown if the interval between

imaging and tissue diagnosis was appropriate (i.e. when comparing imaging signals to

subsequently diagnosed histological glioma grades).

Discussion

Glioma grading

This systematic review has identified 36 research studies, which report on the value of

endogenous CEST techniques to depict brain tumor metabolism. Approximately half of this

research was aimed at predicting glioma histological (WHO) grades. Broadly, these grading

studies indicate a link between greater cellularity in HGGs, higher concentration of proteins

and peptides and APT signal intensity (15, 18). The vast majority of grading research

discovered higher APT image signals in HGGs compared to LGGs, with variable diagnostic

accuracy for individual WHO grade distinction. According to the ROC curve analyses, which produced moderate to high AUC values in a substantial number of studies (13/19), the evidence for the use of CEST in glioma grading is judged to be moderate, whilst the diagnostic accuracy differs amongst glioma grading studies. For example, Zou et al. and Jiang et al. reported AUC values of 0.957 and 1.000, respectively, whereas Zhang et al. and Sakata et al. (2018) achieved 0.723 and 0.760, respectively, for differentiating between HGGs and LGGs using APT. Aside from technical differences and sampling limitations, the heterogeneity in these data sets are likely to be influenced by the lack of glioma grouping according to molecular genetics. A fundamental change has occurred in the reference standard of the WHO classification of CNS Tumors from the previous 2007 version (histological grading only) to the 2016 classification (integrated diagnosis considering histological grading and molecular markers), whereby the majority of CEST studies carried out for glioma grading (17/19) took into account histological findings only. Specifically, lower grade gliomas indistinguishable by histological criteria may differ in malignant potential, for example according to IDH status, which may affect the CEST signal both through difference in the number of solutes – related to the proteasome content – and the pH, depending on the presence or not of an IDH mutation (2, 33). Whilst numerical thresholds from individual studies lacking molecular data should be interpreted with caution, in its entirety the research on glioma grading underscores the potential of CEST to quantify malignant metabolism. This is further supported by the statistical associations between APT metrics and Ki-67 in two prospective research studies (16, 21).

It should be noted that CEST signals contain complex information from various technical factors of which contributions will significantly depend on the experimental setup such as power, length and shape of the RF saturation pulses (24, 26), which may all affect results. A recent meta-analysis by Suh et al. focused on the use of APT for glioma grading

(10) and attributed variations in RF saturation power as a probable factor on the heterogeneity

of study results.

NOE signals, which are hypothesized to originate from magnetization transfer

between water protons and proteins or lipids mediated through intramolecular NOE effects

(9), have been identified as valuable to support glioma characterization. But to which extent

NOE plays a role remains uncertain, with Paech et al observing no significant differences for

glioma WHO grades while Heo et al. reported WHO grade differences for a study of only 10

patients (molecular data unknown). In the study by Paech et al., dns APT had higher

diagnostic performance than conventional APT at 7T MRI, indicating that NOE contributes

to CEST image signal, probably as a confounding effect. Of note, NOE effects are thought to

be substantial at 7T but smaller at 3T clinical field strength (46).

The comparison of APT-CEST with techniques such as DWI, FDG-PET, MRS for

glioma characterization could be of interest for a multimodal diagnostic approach. APT was

reported to provide greater diagnostic accuracy for grading than other techniques, and in the

several studies(13, 15, 17, 22) the combination of CEST with other sequences (IVIM, FDG-

PET and DSC) increased the diagnostic performance. Therefore the utilization of APT

together with other modalities has been proposed to aid grading gliomas. The combination

with APT had been reported that IVIM resulted in the increase of AUC from 0.957 to 0.986

(15), FDG-PET improved the AUC from 0.76 to 0.85 (17), and DSC produced an AUC

increase from 0.877 to 0.923 (22). However, the diagnostic accuracy of the combined use of

APT and MRS has not been comprehensively investigated.

Predicting molecular subtypes of gliomas

Research into the ability of CEST to predict glioma molecular subtypes remains confined to a

small number of studies on IDH and MGMT typing (32, 33). IDH-mutant gliomas

predominantly consist of WHO II-III gliomas and rarely (<10%) of secondary GBM, with an overall better clinical prognosis (1). Distinct from this are IDH wild-type gliomas, many of which correspond to the genetic equivalent of primary glioblastoma with a similarly dismal prognosis, regardless of WHO grade (1). Key disturbances of cellular metabolism, including alterations of amino acid concentrations and reduction of protein expression, are caused by mutations in IDH gene-encoded enzymes (33). In addition, IDH mutations result in accumulation of the oncometabolite 2-hydroxygluterate, which inhibits oxidative phosphorylation and promotes aerobic glycolysis (14). But lactic acidosis due to anaerobic glycolysis in the context of nutrient depletion and growing tumor hypoxia is a key property of IDH^{wt} gliomas, which could confound a pH-based distinction (47). The reported diagnostic accuracy for IDH typing by Jiang et al at 3T (AUC 0.89) and Paech et al at 7T (AUC 0.98, including downfield-rNOE-suppression) is very high. These results are promising with the caveat that no information on blinding to immunohistochemistry is stated for either. Larger studies, including multicenter research on CEST imaging for glioma characterization would be desirable, for example to investigate LGGs, which carry other mutational risk factors for malignant progression (48).

MGMT is a DNA repair enzyme, the activity of which determines glioma susceptibility to alkylating chemotherapy (temozolomide), whereby the methylated MGMT promoter status increases chemosensitivity. Both immunohistochemical MGMT protein expression and MGMT promoter methylation status are prognostic markers of survival in glioma patients (31, 32). With regards to AUC, the results of Su et al. (31) correlating APT signals with MGMT protein expression are similar to those of Jiang et al. (32) assessing MGMT promoter methylation status, but differences in the glioma cohorts and analysis methods limit direct comparability. It has been proposed that MGMT promoter methylation in gliomas produces a decrease of protein expression, which may affect other protein activity

downstream of MGMT (31). Therefore CEST could be considered as a biomarker for

predicting MGMT methylation status, but if sufficient accuracy is achievable to impact

clinical decisions is yet unclear (13).

Paech et al. investigated the comparison of CEST with DWI and DSC for predicting

IDH and MGMT, whereby the diagnostic performance of CEST was reported as marginally

better compared to the others.

The number of studies aimed at predicting glioma molecular subtypes is limited as

yet, meaning that the evidence for CEST in this context, although promising, is uncertain.

Further research is desirable to confirm the method's role in predicting specific genetic

signatures and/or tumor biological behavior.

Diagnosing different type of brain tumors

The study reporting the highest diagnostic accuracy (37) for differentiating PCNSL from

glioblastoma (AUC 0.963) used a parameter not trialed in other research, derived from a

calculation (APT max-min) as opposed to one measurement. However, the result is

noteworthy, possibly reflecting greater APT signal heterogeneity in glioblastoma, which is

known to contain areas of rapid proliferation mixed with (metabolically inactive) necrosis. Of

interest is also the finding of greater APT signal in glioblastoma perilesional tissue compared

to metastases (34), as it raises the possibility that CEST could improve the delineation of MR

imaging-occult glioblastoma infiltration.

Park et al (38) reported adding APT to DSC increased the diagnostic accuracy in

characterizing brain tumors. From this, it is suggested that a multiparametric approach could

be valuable for differentiating malignant gliomas, PCNSL and brain metastatic disease.

The CEST data on the distinction of different types of brain tumors are limited by

small patient numbers (5, 8, 35), different purposes (34, 36-38) and quantitative metrics

presented, so that the evidence supporting CEST for this clinical indication remains

uncertain.

Differentiating recurrence from treatment-related changes

Conventional MRI sequences are unreliable for differentiating treatment-related changes

from tumor recurrence (44) and even using advanced techniques the distinction can be

challenging, meaning there remains an unmet clinical need for a serial imaging method to

provide information on tumor viability. The high reported accuracy in several studies (AUC

0.88-0.98) suggests that APT may dramatically improve the diagnostic value of MRI for this

clinical question. In fact, the performance of APT for differentiating recurrence from

treatment-related changes appears to be higher than for differentiating LGGs and HGGs.

Recurrent tumors include more protein species, whilst there are fewer proteins in regions of

treatment-related changes due to reduced cell density and cytoplasm disruption (49). These

metabolic conditions could explain differences of APT signals between recurrence and

treatment-related changes. Both APT and MET-PET aim to depict endogenous protein

metabolism. Park et al. (42) observed a higher diagnostic accuracy for APT than for 11C

MET-PET, which could be influenced by differences of protein metabolism. APT signal

depends on mobile protein concentration, whilst MET-PET signal originates from actively

synthesized proteins. In addition, methionine accumulation may contribute to disruption of

the blood-brain barrier in HGGs (42). Similar to many studies on the distinction of brain

tumor recurrence from therapy effects, the reference standard in this study included both

cases where the final diagnosis was secured via second look operation and imaging only

follow up (using the Response Assessment in Neuro-Oncology (RANO) criteria).

The evidence for the use of CEST in differentiating recurrence from treatment-related

changes is judged to be weak, with study numbers as the main limitation. Those studies

consistently report positive results and more evidence is required for evaluating the efficacy

of CEST in differentiating recurrence from treatment-related changes.

Therapy response assessment and prognosis prediction

In the post therapy phase, APT may be able depict baseline and dynamic changes in lesion

acidity as a biomarker signature of viable glioblastoma as suggested by Harris et al. (41).

This evidence originates from a single center study and requires validation, particularly as

certain metabolic features of therapy changes and disease recurrence are known to overlap

(50).

In the study following stereotactic radiosurgery, Desmond et al. (40) identified

dynamic changes in normal appearing white matter, which correlated with volume changes in

recently treated brain metastases. As such, CEST signal measurement in normal-appearing

tissue may be of interest to monitor disease progression and disease response.

Given these few studies evaluating the relationships between CEST and therapy

response or prognosis, the evidence in support of this indication is currently uncertain.

In summary, CEST techniques can provide information on brain tumor pathological

metabolism and tissue viability in humans at clinical magnetic field strength. But many

complexities are unresolved. In particular, the current evidence is shaped by a majority of

studies, which solely examined image signals in relation to glioma histological grade, which

limits the clinical impact of this data in the context of the WHO 2016 integrated brain tumor

diagnosis. The heterogeneity of brain tumor cohorts, acquisition and interpretative

approaches is problematic, including a high risk of bias for a substantial proportion of the

published data. From the QUADAS-2 analysis, there was no relationship identifiable between

the severity of bias risk and diagnostic accuracy.

1
2
3
4
5
6
7
8
9
10
11
12
13
14
15
16
17
18
19
20
21
22
23
24
25
26
27
28
29
30
31
32
33
34
35
36
37
38
39
40
41
42
43
44
45
46
47
48
49
50
51
52
53
54
55
56
57
58
59
60

Conclusion

Endogenous CEST imaging offers valuable, potentially unique information in brain tumors, but its diagnostic accuracy is incompletely known. Further research is required to assess the method's role in support of molecular genetic diagnosis, to investigate its use in the post treatment phase, and to compare methods with a view to technical standardization.

References

1.   Lapointe S, Perry A, Butowski NA. Primary brain tumours in adults. Lancet (London, England). 2018;392(10145):432-46.

2.   Louis DN, Perry A, Reifenberger G, et al. The 2016 World Health Organization Classification of Tumors of the Central Nervous System: a summary. Acta neuropathologica. 2016;131(6):803-20.

3.   Al-Okaili RN, Krejza J, Woo JH, et al. Intraaxial brain masses: MR imaging-based diagnostic strategy--initial experience. Radiology. 2007;243(2):539-50.

4.   Thust SC, van den Bent MJ, Smits M. Pseudoprogression of brain tumors. Journal of magnetic resonance imaging : JMRI. 2018.

5.   Jones CK, Schlosser MJ, van Zijl PC, Pomper MG, Golay X, Zhou J. Amide proton transfer imaging of human brain tumors at 3T. Magnetic resonance in medicine. 2006;56(3):585-92.

6.   Kim M, Zaiss, M., Thust, S., Golay, X. Chapter 11; CEST: Chemical Exchange Saturation Transfer. In M. Cercignani, N. Dowell, P. Tofts (Eds.), Quantitative MRI of the Brain Principles of Physical Measurement, Second edition. CRC Press. 2018.

7.   Guivel-Scharen V, Sinnwell T, Wolff SD, Balaban RS. Detection of proton chemical exchange between metabolites and water in biological tissues. Journal of magnetic resonance (San Diego, Calif : 1997). 1998;133(1):36-45.

8.   Shen Y, Xiao G, Shen Z, et al. Imaging of nuclear Overhauser enhancement at 7 and 3 T. NMR in biomedicine. 2017;30(9).

9.   Heo HY, Jones CK, Hua J, et al. Whole-brain amide proton transfer (APT) and nuclear overhauser enhancement (NOE) imaging in glioma patients using low-power steady-state pulsed chemical exchange saturation transfer (CEST) imaging at 7T. Journal of magnetic resonance imaging : JMRI. 2016;44(1):41-50.

10.   Suh CH, Park JE, Jung SC, Choi CG, Kim SJ, Kim HS. Amide proton transfer-weighted MRI in distinguishing high- and low-grade gliomas: a systematic review and meta-analysis. Neuroradiology. 2019;61(5):525-34.

11.   McInnes MDF, Moher D, Thombs BD, et al. Preferred Reporting Items for a Systematic Review and Meta-analysis of Diagnostic Test Accuracy Studies: The PRISMA-DTA Statement. Jama. 2018;319(4):388-96.

12.   Whiting PF, Rutjes AW, Westwood ME, et al. QUADAS-2: a revised tool for the quality assessment of diagnostic accuracy studies. Annals of internal medicine. 2011;155(8):529-36.

13.   Paech D, Windschuh J, Oberhollenzer J, et al. Assessing the predictability of IDH
mutation and MGMT methylation status in glioma patients using relaxation-compensated
multipool CEST MRI at 7.0 T. Neuro-oncology. 2018;20(12):1661-71.

14.   Harris RJ, Yao J, Chakhoyan A, et al. Simultaneous pH-sensitive and oxygen-
sensitive MRI of human gliomas at 3 T using multi-echo amine proton chemical exchange
saturation transfer spin-and-gradient echo echo-planar imaging (CEST-SAGE-EPI). Magnetic
resonance in medicine. 2018;80(5):1962-78.

15.   Zou T, Yu H, Jiang C, et al. Differentiating the histologic grades of gliomas
preoperatively using amide proton transfer-weighted (APTW) and intravoxel incoherent
motion MRI. NMR in biomedicine. 2018;31(1).

16.   Zhang J, Zhu W, Tain R, Zhou XJ, Cai K. Improved Differentiation of Low-Grade
and High-Grade Gliomas and Detection of Tumor Proliferation Using APT Contrast Fitted
from Z-Spectrum. Molecular imaging and biology : MIB : the official publication of the
Academy of Molecular Imaging. 2018;20(4):623-31.

17.   Sakata A, Okada T, Yamamoto Y, et al. Addition of Amide Proton Transfer Imaging
to FDG-PET/CT Improves Diagnostic Accuracy in Glioma Grading: A Preliminary Study
Using the Continuous Net Reclassification Analysis. AJNR American journal of
neuroradiology. 2018;39(2):265-72.

18.   Togao O, Hiwatashi A, Yamashita K, et al. Grading diffuse gliomas without intense
contrast enhancement by amide proton transfer MR imaging: comparisons with diffusion-
and perfusion-weighted imaging. European radiology. 2017;27(2):578-88.

19.   Su C, Liu C, Zhao L, et al. Amide Proton Transfer Imaging Allows Detection of
Glioma Grades and Tumor Proliferation: Comparison with Ki-67 Expression and Proton MR
Spectroscopy Imaging. AJNR American journal of neuroradiology. 2017;38(9):1702-9.

20.   Sakata A, Fushimi Y, Okada T, et al. Diagnostic performance between contrast
enhancement, proton MR spectroscopy, and amide proton transfer imaging in patients with
brain tumors. Journal of magnetic resonance imaging : JMRI. 2017;46(3):732-9.

21.   Jiang S, Eberhart CG, Zhang Y, et al. Amide proton transfer-weighted magnetic
resonance image-guided stereotactic biopsy in patients with newly diagnosed gliomas.
European journal of cancer (Oxford, England : 1990). 2017;83:9-18.

22.   Choi YS, Ahn SS, Lee SK, et al. Amide proton transfer imaging to discriminate
between low- and high-grade gliomas: added value to apparent diffusion coefficient and
relative cerebral blood volume. European radiology. 2017;27(8):3181-9.

23.   Bai Y, Lin Y, Zhang W, et al. Noninvasive amide proton transfer magnetic resonance
imaging in evaluating the grading and cellularity of gliomas. Oncotarget. 2017;8(4):5834-42.

24. Togao O, Hiwatashi A, Keupp J, et al. Amide Proton Transfer Imaging of Diffuse Gliomas: Effect of Saturation Pulse Length in Parallel Transmission-Based Technique. PloS one. 2016;11(5):e0155925.

25. Park JE, Kim HS, Park KJ, Kim SJ, Kim JH, Smith SA. Pre- and Posttreatment Glioma: Comparison of Amide Proton Transfer Imaging with MR Spectroscopy for Biomarkers of Tumor Proliferation. Radiology. 2016;278(2):514-23.

26. Harris RJ, Cloughesy TF, Liau LM, et al. Simulation, phantom validation, and clinical evaluation of fast pH-weighted molecular imaging using amine chemical exchange saturation transfer echo planar imaging (CEST-EPI) in glioma at 3 T. NMR in biomedicine. 2016;29(11):1563-76.

27. Sakata A, Okada T, Yamamoto A, et al. Grading glial tumors with amide proton transfer MR imaging: different analytical approaches. Journal of neuro-oncology. 2015;122(2):339-48.

28. Togao O, Yoshiura T, Keupp J, et al. Amide proton transfer imaging of adult diffuse gliomas: correlation with histopathological grades. Neuro-oncology. 2014;16(3):441-8.

29. Zhou J, Zhu H, Lim M, et al. Three-dimensional amide proton transfer MR imaging of gliomas: Initial experience and comparison with gadolinium enhancement. Journal of magnetic resonance imaging : JMRI. 2013;38(5):1119-28.

30. Zhou J, Blakeley JO, Hua J, et al. Practical data acquisition method for human brain tumor amide proton transfer (APT) imaging. Magnetic resonance in medicine. 2008;60(4):842-9.

31. Su L, Gao P, Lin S, et al. Predicting O6-Methylguanine-DNA Methyltransferase Protein Expression in Primary Low- and High-Grade Gliomas Using Certain Qualitative Characteristics of Amide Proton Transfer-Weighted Magnetic Resonance Imaging. World neurosurgery. 2018;116:e814-e23.

32. Jiang S, Rui Q, Wang Y, et al. Discriminating MGMT promoter methylation status in patients with glioblastoma employing amide proton transfer-weighted MRI metrics. European radiology. 2018;28(5):2115-23.

33. Jiang S, Zou T, Eberhart CG, et al. Predicting IDH mutation status in grade II gliomas using amide proton transfer-weighted (APTw) MRI. Magnetic resonance in medicine. 2017;78(3):1100-9.

34. Yu H, Lou H, Zou T, et al. Applying protein-based amide proton transfer MR imaging to distinguish solitary brain metastases from glioblastoma. European radiology. 2017;27(11):4516-24.

35.   Khlebnikov V, Polders D, Hendrikse J, et al. Amide proton transfer (APT) imaging of brain tumors at 7 T: The role of tissue water T1 -Relaxation properties. Magnetic resonance in medicine. 2017;77(4):1525-32.

36.   Jeong HK, Han K, Zhou J, et al. Characterizing amide proton transfer imaging in haemorrhage brain lesions using 3T MRI. European radiology. 2017;27(4):1577-84.

37.   Jiang S, Yu H, Wang X, et al. Molecular MRI differentiation between primary central nervous system lymphomas and high-grade gliomas using endogenous protein-based amide proton transfer MR imaging at 3 Tesla. European radiology. 2016;26(1):64-71.

38.   Park JE, Kim HS, Park KJ, Choi CG, Kim SJ. Histogram Analysis of Amide Proton Transfer Imaging to Identify Contrast-enhancing Low-Grade Brain Tumor That Mimics High-Grade Tumor: Increased Accuracy of MR Perfusion. Radiology. 2015;277(1):151-61.

39.   Regnery S, Adeberg S, Dreher C, et al. Chemical exchange saturation transfer MRI serves as predictor of early progression in glioblastoma patients. Oncotarget. 2018;9(47):28772-83.

40.   Desmond KL, Mehrabian H, Chavez S, et al. Chemical exchange saturation transfer for predicting response to stereotactic radiosurgery in human brain metastasis. Magnetic resonance in medicine. 2017;78(3):1110-20.

41.   Harris RJ, Cloughesy TF, Liau LM, et al. pH-weighted molecular imaging of gliomas using amine chemical exchange saturation transfer MRI. Neuro-oncology. 2015;17(11):1514-24.

42.   Park JE, Lee JY, Kim HS, et al. Amide proton transfer imaging seems to provide higher diagnostic performance in post-treatment high-grade gliomas than methionine positron emission tomography. European radiology. 2018;28(8):3285-95.

43.   Mehrabian H, Desmond KL, Soliman H, Sahgal A, Stanisz GJ. Differentiation between Radiation Necrosis and Tumor Progression Using Chemical Exchange Saturation Transfer. Clinical cancer research : an official journal of the American Association for Cancer Research. 2017;23(14):3667-75.

44.   Park KJ, Kim HS, Park JE, Shim WH, Kim SJ, Smith SA. Added value of amide proton transfer imaging to conventional and perfusion MR imaging for evaluating the treatment response of newly diagnosed glioblastoma. European radiology. 2016;26(12):4390-403.

45.   Ma B, Blakeley JO, Hong X, et al. Applying amide proton transfer-weighted MRI to distinguish pseudoprogression from true progression in malignant gliomas. Journal of magnetic resonance imaging : JMRI. 2016;44(2):456-62.

46.   Zhou J, Hong X, Zhao X, Gao JH, Yuan J. APT-weighted and NOE-weighted image contrasts in glioma with different RF saturation powers based on magnetization transfer ratio asymmetry analyses. Magnetic resonance in medicine. 2013;70(2):320-7.

47.   Khurshed M, Molenaar RJ, Lenting K, Leenders WP, van Noorden CJF. In silico gene expression analysis reveals glycolysis and acetate anaplerosis in IDH1 wild-type glioma and lactate and glutamate anaplerosis in IDH1-mutated glioma. Oncotarget. 2017;8(30):49165-77.

48.   Korshunov A, Casalini B, Chavez L, et al. Integrated molecular characterization of IDH-mutant glioblastomas. Neuropathology and applied neurobiology. 2019;45(2):108-18.

49.   Zhang P, Guo Z, Zhang Y, et al. A preliminary quantitative proteomic analysis of glioblastoma pseudoprogression. Proteome science. 2015;13:12.

50.   Zhang H, Ma L, Wang Q, Zheng X, Wu C, Xu BN. Role of magnetic resonance spectroscopy for the differentiation of recurrent glioma from radiation necrosis: a systematic review and meta-analysis. European journal of radiology. 2014;83(12):2181-9.

Figure 1. Flow chart describing the study selection process. Two studies contained data on glioma grading and predicting molecular subtypes, and one study was assigned to both glioma grading and differentiating recurrence from treatment-related changes.

Figure 2. Results of the QUADAS2 quality assessment of the included studies. The risk of bias in four different domains and concerns regarding applicability in three domains are shown.

1
2
3
4
5
6
7
8
9
10
11
12
13
14
15
16
17
18
19
20
21
22
23
24
25
26
27
28
29
30
31
32
33
34
35
36
37
38
39
40
41
42
43
44
45
46
47
48
49
50
51
52
53
54
55
56
57
58
59
60

Supplementary material 1.

Search was performed in 19/11/2018.

Search strategy in PubMed: 174 articles

(((((((((((brain tumour[tw]) OR brain tumor[tw]) OR glioma[tw]) OR brain metastasis[tw])

OR astrocytoma[tw]) OR oligodendroglioma[tw]) OR brain neoplasm[tw]) OR brain

cancer[tw]) OR glioblastoma[tw]) OR brain neoplasm[MeSH Terms]) OR glioma[MeSH

Terms]) AND (((((((((((magnetic resonance imaging[MeSH Terms]) AND CEST[tw]) OR

chemical exchange saturation transfer[tw]) OR APT[tw]) OR amide proton transfer[tw]) OR

magnetization transfer[tw]) OR z-spectrum[tw]) OR chemical exchange[tw]) OR exchange

transfer[tw]) OR saturation transfer[tw]) OR nuclear overhauser effect[tw]) AND

Humans[Mesh]

Search strategy in EMBASE: 240 articles

1. (brain tumor or brain tumour or glioma or brain metastasis or astrocytoma or

oligodendroglioma or brain neoplasm or brain cancer or glioblastoma).af.

2. magnetic resonance imaging.af.

3. (CEST or chemical exchange saturation transfer or APT or amide proton transfer or

magnetization transfer or z-spectrum or chemical exchange or exchange transfer or saturation

transfer or nuclear overhauser effect).af.

4. 1 and 2 and 3

5. limit 4 to human

1
2
3
4
5
6
7
8
9
10
11
12
13
14
15
16
17
18
19
20
21
22
23
24
25
26
27
28
29
30
31
32
33
34
35
36
37
38
39
40
41
42
43
44
45
46
47
48
49
50
51
52
53
54
55
56
57
58
59
60

Search strategy in the Cochrane Library: 16 articles

#1   brain tumour

#2   brain tumor

#3   glioma

#4   brain metastasis

#5   brain neoplasm

#6   brain cancer

#7   glioblastoma

#8   astrocytoma

#9   oligodendroglioma

#10   #1 or #2 or #3 or #4 or #5 or #6 or #7 or #8 or #9

#11   CEST or "chemical exchange saturation transfer" or APT or "amide proton transfer"

or "magnetization transfer" or z-spectrum or "chemical exchange" or "exchange transfer" or

"saturation transfer" or "nuclear overhauser effect"

#12   magnetic resonance imaging

#13   #10 and #11 and #12

Supplementary Table 1. Details of MR imaging parameters for all included studies

Author, year	CEST technique	Saturation duration	Saturation power	Frequency offsets	Total scan time	Method of correcting B0 field inhomogeneity	MRI field strength/ manufacturer
Grading gliomas							
Paech 2018	APT, NOE (2D, single slice, gradient echo)	pulse width = 15 ms, duration time = 10 ms, duty cycle = 60%, saturation time = 3.75 s	2 different B1 amplitudes (1.0 µT and 0.6 µT)	65 unevenly sampled saturation offsets Frequency offsets were distributed with higher sampling around the CEST pools: ±4 ppm to ±3 ppm in steps of 0.1 ppm, from ±2.75 ppm to ±2 ppm in steps of 0.25 ppm, and ±1.8 ppm to ±1.2 ppm in steps of 0.1 ppm, ±0.5 ppm, ±0.25 ppm, and 0 ppm.	11min	Simultaneous mapping of water shift and B1 (WASABI) (1)	7T Siemens
Harris 2018	Amine proton CEST spin-and-gradient echo (SAGE) echo planar imaging (EPI) (25 contiguous slices, 4 mm slice thickness)	3 x 100 ms Gaussian pulses	6µT	A total of 29 z-spectral points were acquired with data around ± 3.0ppm and 0.0 ppm with respect to water (from -3.5 to -2.5 in intervals of 0.1; from -0.3 to +0.3 in intervals of 0.1; and from +2.5 to +3.5 in intervals of 0.1).	7 min 30 s	Water saturation shift referencing (WASSR) (2)	3T Siemens
Zou 2018	APT (2D, single slice, turbo-spin-echo pulse sequence)	4 x 200 ms with 10 ms inter-pulse delay	2µT	Multi-offset [31 off-sets: 0, ±0.25, ±0.5, ±0.75, ±1, ±1.5, ±2, ±2.5, ±3 (2), ±3.25 (4), ±3.5 (8), ±3.75 (4), ±4 (2), ±4.5, ±5, ±6 ppm; the values in parentheses are the number of acquisitions (which was one, if not specified).	3 min 12 s	To determine field inhomogeneity effects on z-spectra, the measured z-spectrum for each voxel was interpolated to 2049 points and shifted along the direction of the offset axis to correspond to 0 ppm at its lowest intensity. (3)	3T Philips
Zhang 2018	APT (an axial brain slice)	400 ms	2µT	A total of 33 images acquired at various saturation offsets, including + 15.6, ± 6, ± 5, ± 4.5, ±4, ± 3.75, ± 3.5, ± 3.25, ± 3, ± 2.5, ± 2, ± 1.5, ± 1, ± 0.75, ±0.5, ± 0.25, 0, and + 39.1 ppm	3 min 18 s	Conventional APT was corrected for B0 inhomogeneity according to the ΔB0 map produced (4).	3T GE
Sakata 2018	APT (prototype 3D gradient-echo pulse sequence)	3 x 100 ms duration with 100 ms interpulse delay	2µT	18 consecutive datasets were acquired with different offset frequencies Δω (0,±0.6,±1.2,±1.8,±2.4,±3.0,±3.6,±4.2 and ±4.8 ppm) from the bulk water resonance.	unclear	To correct for inhomogeneities of the static magnetic field, spline interpolation was applied to determine the minimum of the z-spectrum, which was then set to offset-frequency δ=0.(5)	3T Siemens
Togao 2017	APT (2D, single slice)	40 × 50 ms, sinc-gauss-shaped elements	2µT.	25 saturation frequency offsets from ω=−6 to +6 ppm with a step of 0.5 ppm as well as one far-off-resonant frequency (ω=−1560 ppm) for signal normalization	2 min 20 s	A ΔB0 map for off-resonance correction was acquired separately using a 2D gradient-echo with identical spatial resolution for a point-by-point ΔB0 correction. The local B0 field shift in Hz was obtained from the B0 map, which was created from dual echo gradient echo images (ΔTE=1 msec), and each voxel was corrected in image intensity for the nominal saturation frequency offset by Lagrange	3T Philips

						interpolation among the neighboring Z-spectral images.	
Su 2017	APT (single slice)	400 ms.	2µT	Data were acquired with 2NEX in a saturation frequency list of 15.6, ±6, ±5, ±4.5, ±4, ±3.75,±3.5,±3.25,±3,±2.5,±2,±1.5,±1,±0.75,±0.5,±0.25, and 0 ppm and 1 no-saturation map, resulting in 66 images.	3 min 18 s	B0 correction was performed by shifting the minimum signal of the z spectrum to 0 Hz.	3T GE
Sakata 2017	APT (2D, single slice)	25 x 40 ms with 1ms interval	1µT	MT spectra over an offset range of ±10ppm with a step size of 0.5ppm with respect to water resonance were obtained.	6 min 9 s	The minimum value for MT spectra obtained from APT imaging was estimated from the original data by spline interpolation with Lorentzian function fitting, and displacement from the water resonance frequency owing to B0-field inhomogeneity was corrected.	3T Toshiba
Jiang 2017_2	APT (3D gradient- and spin-echo image acquisition)	4x200 ms	2µT	APTw imaging was acquired with a six-offset protocol (S0, ±3, ±3.5, ±4 ppm from water; 1, 1, 4, 1 averages, respectively), which was acquired twice and averaged during data processing.	10 min 42 s	WASSR	3T Philips
Choi 2017	APT (3D gradient- and spin-echo image acquisition)	4 x 200 ms	2 µT	Four repetitions at six saturation-frequency offsets (±3.0, ±3.5 and ±4.0 ppm)	7 min 36 s	WASSR	3T Philips
Bai 2017	APT (2D, single slice, gradient echo)	995 ms (The length of the each saturation radiofrequency pulse was 99 ms, and the gap between the pulses was 100 ms.)	2µT.	21 frequency offsets from -5 to +5 ppm with even intervals of 0.5 ppm	1 min 45 s per single slice	The B0 field inhomogeneity was calculated according to the deviation of the minimum of the fitted curve from 0 ppm.	3T Siemens
Togao 2016	APT (2D, single slice)	10 x 50 ms, 20 x 50 ms, 40 x 50 ms	2µT	25 saturation frequency offsets from ω = −6 to +6 ppm with a step of 0.5 ppm as well as one far off-resonant frequency (ω = −1560 ppm) for signal normalization	2 min 20 s for one Z-spectrum	A B0 map for off-resonance correction was acquired separately using a 2D gradient-echo with identical spatial resolution, and it was used for a point-by-point B0 correction. A dedicated plug-in was build to analyze the Z-spectra and asymmetry of magnetization transfer ratio (MTRasym) equipped with a correction function for B0 inhomogeneity as previously demonstrated(6).	3T Philips
Park 2016_2	APT (3D gradient-echo multishot echo-planar imaging)	70 ms, limiting the repetition time to 140 ms	1 µT	(Δω ppm = ± 5.0 ppm, where Δω is the frequency of amide and water exchange site) with respect to water, and a step size of 0.36 ppm. A total of 29 off-resonance sequences and one additional far off resonance	8 min 50 s	The minimum of the APT z-spectra was estimated from the original data, and the displacement from the water resonance frequency was corrected. A shifted offset frequency axis for each of z-spectrum	3T Philips

				acquisition for normalization of the APT MR imaging signals		was generated in our study with cases of relatively large spectral shift, to retain the whole spectral points at each voxel rather than discarding quite a few points because of field inhomogeneity.	
Heo 2016	APT, NOE (3D multishot gradient-echo sequence)	25 ms	1µT peak amplitude, 0.54µT average power	Following two dummy scans, 75 volumes at saturation frequency off-sets were acquired: off (S0 image), off, -18, -14, -12, -10, -8, off, -7, -5, -4.7, -4.5, off, -4.3, -4.1, -3.9, -3.7, -3.5, off,-3.3,-3.1,-2.9,-2.7,-2.5, off,-2.0,-1.8,-1.6,-1.4,-1.2, off,-1.0,-0.8,-0.6, -0.4,-0.2, off, 0, 0.2, 0.4, 0.6, 0.8, off, 1.0, 1.2, 1.4, 1.6, 1.8, off, 2.0, 2.5, 2.7, 2.9, 3.1, off, 3.3, 3.5, 3.7, 3.9, 4.1, off, 4.3, 4.5, 4.7, 5.0, 7.0, off, 8.0, 10.0, 12.0, 14.0, 18.0ppm (relative to the water resonance), off, and off.	13min	A Lorentzian curve fit was used to correct for B0 field inhomogeneity effects. The Z-spectra were interpolated with the interval step of 0.01ppm and aligned correspondingly on a pixel-by-pixel basis with the water frequency in each voxel at 0 ppm.	7T Philips
Harris 2016	pH weighted amine CEST-EPI	3x 100 ms Gaussian pulses	6µT	Unclear	5 min	Unclear	3T Siemens
Sakata 2015	APT (3D gradient-echo pulse sequence)	3 x 100 ms duration with 100 ms interpulse delay	2µT	Δω (0, ±0.6, ±1.2, ±1.8, ±2.4, ±3.0, ±3.6, ±4.2, and ±4.8 ppm) from the bulk water resonance	5min 31s	The APTasym at 3.5 ppm was obtained after linear interpolation between the originally sampled points to a resolution of 0.1 ppm and subsequent correction for inhomogeneity of the static magnetic field by Z-spectrum shifting. (5)	3T Siemens
Togao 2014	APT (2D, single slice)	40 x 50 ms, sinc-gauss-shaped elements	2µT	25 saturation frequency offsets from ω=-6 to +6 ppm with a step of 0.5 ppm as well as 1 far off-resonant frequency (ω=-160 ppm) for signal normalization	2 min 20 s for one Z-spectrum	A ΔB0 map for off-resonance correction was acquired separately using a 2D gradient echo with identical spatial resolution, and it was used for a point-by-point ΔB0 correction.	3T Philips
Zhou 2013	APT (3D gradient- and spin-echo image acquisition)	4 x 200 ms duration, each followed by a crusher gradient of 10 ms duration and 10 mT/m strength	2µT	A six-offset protocol (S0, ±3, ±3.5, ±4 ppm from water; 1, 1, 4, 1 averages, respectively)	10 min 42 s	WASSR	3T Philips
Zhou 2008	APT (A single-slice turbo spin echo (TSE) imaging readout with a sensitivity encoding (SENSE) factor of 2 and a TSE factor of 32)	500 ms	4µT	Six frequency offsets (namely, ±3, ±3.5, and ±4 ppm) In an extra scan, a z-spectrum was acquired (33 offsets from 8 to –8 ppm with intervals of 0.5 ppm, one average)	2 min 48 s (saturated image) 1 min 42 s	To determine the field inhomogeneity effects on z-spectra, the measured z-spectrum for each voxel was interpolated to 2049 points and shifted along the direction of the offset axis to correspond to 0 ppm at its lowest intensity.	3T Philips

						(unsat urated)	
Predicting molecular subtypes							
Harris 2018	Amine proton CEST echo spin-and-gradient echo (SAGE) EPI (25 contiguous slices with a 4-mm slice thickness)	3 x 100 ms Gaussian pulses	6µT	A total of 29 z-spectral points were acquired with data around ± 3.0ppm and 0.0 ppm with respect to water (from -3.5 to -2.5 in intervals of 0.1; from -0.3 to +0.3 in intervals of 0.1; and from +2.5 to +3.5 in intervals of 0.1).	7 min 30 s	WASSR	3T Siemens
Su 2018	APT (2D, single slice, single-shot, fast spin-echo pulse sequence)	400 ms	2µT	49 offsets =±6, ±5.75, ±5.5, ±5.25, ±5,±4.75, ±4.5, ±4.25, ±4, ±3.75, ±3.5, ±3.25, ±3, ±2.75, ±2.5,±2.25, ±2, ±1.75, ±1.5, ±1.25, ±1, ±0.75, ±0.5, ±0.25, 0 ppm and 3 unsaturated map acquired) with 0.56 number of excitations was used, resulting in 52 images.	134s	B0 correction was done by shifting the minimum signal of the z spectrum to 0 Hz.	3T GE
Jiang 2018	APT (2D, single slice, fast spin-echo pulse sequence)	800 ms	2µT	Six-offset APT data acquisition (±3, ±3.5, ±4 ppm, 8 signal averages), together with a separately acquired z spectrum (33 offsets from 8 to -8 ppm with intervals of 0.5 ppm, one average) (Wen Z, et al. Neuroimage 2010;51:616-622)	unclear	Unclear. Z spectrum was corrected for the B0 inhomogeneity effect on a voxel-by-voxel basis.	3T Philips
Paech 2018	APT, NOE (2D, single slice)	Pulse width = 15 ms, duration time = 10 ms, duty cycle = 60%, saturation time = 3.75 s	2 different B1 amplitudes (1.0 µT and 0.6 µT)	65 unevenly sampled saturation offsets. Frequency offsets were distributed with higher sampling around the CEST pools:±4 ppm to±3 ppm in steps of 0.1 ppm, from ±2.75 ppm to ±2 ppm in steps of 0.25 ppm, and ±1.8 ppm to ±1.2 ppm in steps of 0.1 ppm, ±0.5 ppm, ±0.25 ppm, and 0 ppm.	11 min	WASABI	7T Siemens
Jiang 2017_1	APT, MT (2D, single slice, single-shot, fast spin-echo pulse sequence)	4 x 200 ms	2µT	31 offsets=0, ± 0.25, ± 0.5, ± 0.75, ± 1, ± 1.5, ± 2, ± 2.5, ± 3 (2), ± 3.25 (4), ± 3.5 (8), ± 3.75 (4), ± 4 (2), ± 4.5, ± 5, ± 6 ppm; the values in parentheses were the number of acquisitions, which was 1, if not specified	3 min	To determine the field inhomogeneity effects on z-spectra, the measured z-spectrum for each voxel was interpolated to 2049 points and shifted along the direction of the offset axis to correspond to 0 ppm at its lowest intensity. (3)	3T Philips
Diagnosing different type of brain tumors							
Yu 2017	APT (2D)	Duration time =800 ms; inter-pulse delay =10 ms	2µT	Multi-offset (offsets =0, ±0.25, ±0.5, ±0.75, ±1, ±1.5, ±2, ±2.5, ±3, ±3.25, ±3.5, ±3.75, ±4, ±4.5, ±5 and ±6 ppm)	192 s	The B0 field inhomogeneity effect was corrected. (7)	3T Philips
Shen 2017	APT, NOE (MT-prepared gradient echo sequence)	A 20 ms width Fermi pulse, the total saturation time is 5.12 s	0.6µT	49 equidistant frequency offsets between 6 and −6 ppm and an additional S0 image were acquired	unclear	WASSR	3T GE

Khlebnikov 2017	APT (A pulsed 3D steady-state CEST sequence)	50 ms rectangular-shaped pulse followed by a 50 mT/m spoiler of 25 ms	1.8µT	17 frequency offset (Hz) pairs: 0, ±75, ±150, ±800, ±900, ±1000, ±1100, ±1200, and±5000.	6 min 40 s	WASSR	7T Philips
Jeong 2017	APT (3D gradient- and spin-echo sequence)	4 x 200 ms	2µT	6 saturation frequency offsets (±3.0, ±3.5, and ±4.0 ppm)	7 min 36 s	WASSR	3T Philips
Jiang 2016	APT (fast spin-echo pulse sequence)	4 x 200 ms	2µT	31 offsets=0, ± 0.25, ± 0.5, ± 0.75, ± 1, ± 1.5, ± 2, ± 2.5, ± 3 (2), ± 3.25 (4), ± 3.5 (8), ± 3.75 (4), ± 4 (2), ± 4.5, ± 5, ± 6 ppm; the values in parentheses were the number of acquisitions, which was 1, if not specified. The total CEST signal intensity (CESTtotal) was defined as the integral of the whole MTRasym spectrum between 0 and 5 ppm	3 min	To determine the field inhomogeneity effects on z-spectra, the measured z-spectrum for each voxel was interpolated to 2049 points and shifted along the direction of the offset axis to correspond to 0 ppm at its lowest intensity.(3)	3T Philips
Park 2015	APT (3D gradient-echo with multishot echo-planar imaging)	70 msec, limiting the repetition time to 140 msec	1 µT	($\Delta\omega$ ppm = ± 5.0 ppm, where $\Delta\omega$ is the frequency of amide and water exchange site) with respect to water, and a step size of 0.36 ppm. A total of 29 off-resonance sequences and one additional far off resonance acquisition for normalization of the APT MR imaging signals.	8 min 50 s	The minimum of the APT z-spectrum was estimated from the original data, and the displacement from the water resonance frequency owing to B0 field inhomogeneity was corrected.	3T Philips
Jones 2006	APT	3 s	3µT	Two patients were scanned using 33 offsets from-8 to 8 ppm with an interval of 0.5 ppm to verify the offset dependence of the proton transfer effects. The other eight patients were scanned at two offsets (±3.5 ppm relative to the water frequency) and with eight averages to increase the SNR.	10 min	The minimum of the fitted curve was assumed to be the on-resonance water frequency and was shifted to be 0 ppm.	3T Philips
Differentiating recurrence from treatment-related changes							
Park 2018	APT (3D turbo spin-echo imaging sequence)	40 x 50 ms	2 µT	9 acquisitions [−2.7, +2.7, −3.5, +3.5 (3 acquisitions at different echo times, TEs), −4.3, +4.3, −1560 ppm]	7 min 5 s	B0 correction was performed. A B0 map for off-resonance corrections was estimated from the data acquired at three different TEs (TE = ± 0.4 ms) using an iterative filtering and mapping procedure with spatial smoothing, three-point Dixon method.	3T Philips
Mehrabian 2017	APT, MT, NOE (A single-shot echo planar imaging sequence)	4 x 242.5 ms	0.52 µT	Offset frequencies between -750Hz(-5.9ppm) and 750Hz (5.9ppm) at 25Hz increments. Four reference offsets of 100 kHz (~780 ppm) were acquired at the beginning, and another four reference images were acquired at the end of the spectrum.	8.75 min	Fitting a Lorentzian line-shape to the data points surrounding the direct effect (offset < 1.3 ppm) and the end tails of the spectrum (offset > 4.5 ppm). The spectrum was then shifted so that the minimum was at 0 Hz, and the spectrum was resampled at the same offset frequencies as the imaging protocol.	3T Philips

Park 2016_2	APT (3D gradient-echo multishot echo-planar imaging)	70 ms, limiting the repetition time to 140 ms	1 µT	(Δω ppm = ± 5.0 ppm, where Δω is the frequency of amide and water exchange site) with respect to water, and a step size of 0.36 ppm a total of 29 off-resonance sequences and one additional far off resonance acquisition for normalization of the APT MR imaging signals.	8 min 50 s	The minimum of the APT z-spectra was estimated from the original data and the displacement from the water resonance frequency was corrected. A shifted offset frequency axis for each of z-spectrum was generated in our study with cases of relatively large spectral shift, to retain the whole spectral points at each voxel rather than discarding quite a few points because of field inhomogeneity.	3T Philips
Park 2016_1	APT (3D gradient-echo echo planar imaging)	70 ms	1 µT	from −5.0 ppm to +5.0 ppm at a stepsize of 0.37 ppm with respect to water resonance. A total of 29 off-resonance scans and one additional far off-resonance scan for normalization of the APT MR signals.	8 min 50 s	The APT z-spectrum was more precisely corrected for the B0-inhomogeneity-induced spectral shift using the spectral minimum of the direct water saturation component derived from the following; APT z-spectra from each voxel were interpolated to 1 Hz step-size and fit to a 3-pool model which characterizes the direct water saturation, the asymmetrical (Δω=-2.5 ppm) solid-phase magnetization transfer (MT) component and the APT (Δω=3.5 ppm) component.	3T Philips
Ma 2016	APT (3D gradient-and spin-echo image acquisition)	4 x 200 ms	2µT	unsaturated S0,63,63.5,64ppm from water; 1, 1, 4, 1 averages, respectively).	10 min 42 s	The B0 inhomogeneity effect was corrected using the determined B0 map from the water saturation shift-referencing method.	3T Philips
Therapy response assessment							
Regnery 2018	NOE, APT (2D gradient echo sequence)	Pulse width = 15 ms, duration time = 10 ms, duty cycle = 60%, saturation time = 3.75 s	Two distinct B1 amplitudes 1.0 µT and 0.6 µT	Offsets unknown (MTRasym was calculated at 3.5 ppm)	22–25 min	WASABI	7T Siemens
Desmond 2017	APT, NOE, MT, amine (2D, echo planar imaging)	3 x 250 ms	0.52 µT	Every 25Hz between −750 and 750Hz (~±6 parts per million [ppm]) and with a reference image at 100 kHz (~1,500ppm) for a total of 64 offset frequencies	12 min	B0 inhomogeneities were corrected by fitting a Lorentzian function to the data points in a region surrounding the minimum of the direct effect, and then the CEST data were shifted so that the minimum of the fitted function was at 0 Hz.	3T Philips
Harris 2015	Amine CEST	3 x 100 ms	6µT	A total of 1 to 5 slices of CEST images with varying z-spectral points ranging from 5 to 51 and from 25.0 ppm to +5.0 ppm were acquired. For biopsy patients, 3 slices were acquired through the largest extent of the tumor using spectral points acquired at 0, +0.125, +0.25, +0.375, +0.5, +2.5, +2.75, +3.0, +3.25, and +3.5 ppm, rather than a full z-spectrum with a single slice.	unclear	WASSR	3T Siemens

References

1.   Schuenke P, Windschuh J, Roeloffs V, Ladd ME, Bachert P, Zaiss M. Simultaneous mapping of water shift and B1 (WASABI)-

Application to field-Inhomogeneity correction of CEST MRI data. Magnetic resonance in medicine. 2017;77(2):571-80.

2.   Kim M, Gillen J, Landman BA, Zhou J, van Zijl PC. Water saturation shift referencing (WASSR) for chemical exchange saturation

transfer (CEST) experiments. Magnetic resonance in medicine. 2009;61(6):1441-50.

3.   Zhou J, Blakeley JO, Hua J, et al. Practical data acquisition method for human brain tumor amide proton transfer (APT) imaging.

Magnetic resonance in medicine. 2008;60(4):842-9.

4.   Cai K, Haris M, Singh A, et al. Magnetic resonance imaging of glutamate. Nature medicine. 2012;18(2):302-6.

5.   Schmitt B, Zaiss M, Zhou J, Bachert P. Optimization of pulse train presaturation for CEST imaging in clinical scanners. Magnetic

resonance in medicine. 2011;65(6):1620-9.

6.   Togao O, Yoshiura T, Keupp J, et al. Amide proton transfer imaging of adult diffuse gliomas: correlation with histopathological grades.

Neuro-oncology. 2014;16(3):441-8.

7.   Wen Z, Hu S, Huang F, et al. MR imaging of high-grade brain tumors using endogenous protein and peptide-based contrast. Neuroimage.

2010;51(2):616-22.

Supplementary Table 2. The characteristics of the included studies for glioma grading

Author, year	Main research purpose	CEST technique	Other Imaging	Total N	Histology	Age (mean ±SD, range)	ROI method	Key parameter	Parameter value	P value	Cut off value	Sens	Spec	AUC	Additional results
Paech 2018 Germany Prospective	To investigate the non-invasive predictability of IDH mutation status, MGMT promoter methylation, and differentiation of LGG and HGG.	APT, NOE	ADC, rCBV	31	6 low grade 25 high grade	27-86	Whole lesion T1WI+C, T2WI	NOE mean	LGG 7.69 ± 3.96 % HGG 9.06 ± 3.21 %	P=0.24	8.95	61	83	0.66	rCBV AUC 0.73, ADC mean 0.53
								NOE 10th pc	LGG 4.24 ± 2.59 % HGG 4.22 ± 2.01 %	P=1.00	5.18	33	83	0.5	
								APT mean	LGG 3.07 ± 1.50 % HGG 3.96 ± 1.32 %	P=0.07	3.66	79	80	0.76	
								APT 90th pc	LGG 4.54 ± 2.15 % HGG 6.03 ± 2.26 %	P=0.11	5.42	67	80	0.73	
								downfield-rNOE-suppressed (dns)-APT mean	LGG 1.47 ± 0.68 % HGG 2.14 ± 0.85 %	P=0.0497	1.88	71	100	0.78	
								dns-APT 90th pc	LGG 2.37 ± 1.20 % HGG 4.01 ± 1.85 %	P=0.0234	3.62	63	100	0.83	
Harris 2018 USA Unclear	To introduce a new pH- and oxygen-sensitive MRI technique using amine proton CEST echo spin-and-gradient echo (SAGE) EPI.	Amine CEST	NA	47	13 grade II 14 grade III 20 grade IV (including 26 recurrent tumor)	54.6 ± 16.1, 22-82	Whole FLAIR lesion, T1WI CE (grade IV), also VOI NAWM	median MTR asym at 3.0 ppm	grade II (1.5± 0.1%) grade III (1.6 ±0.2%) grade IV (2.0± 0.2%)	II vs III P>0.05 II vs IV P=0.0432 III vs IV P>0.05	NA	NA	NA	NA	
								median R2'	grade II=4.6 ± 0.4 sec^{-1} grade III=4.2 ± 0.4 sec^{-1} grade IV=5.4 ± 0.3 sec^{-1}	ANOVA, P=0.0537	NA	NA	NA	NA	
Zou 2018 China Prospective	To investigate the diagnostic performance	APT	IVIM	51	26 grade II 14 grade III 11 grade IV	female: 38.1 ± 13.4;	hot spot (five small	MTR asym (APTW)	HGG 2.77 ± 0.35 % grade II 1.98 ± 0.58 %	LGG vs HGG P<0.001	>2.34	100	88.5	LGG vs HGG 0.935	IVIM parameters (diffusion coefficient and perfusion

Study	Purpose	Technique	Other	N	Grades	Age	ROI	Parameter	Values	P	Ratio/Cutoff	Sens	Spec	AUC	Conclusion
of APT and IVIM in grading gliomas						18–63 male: 42.9 ± 14.3; 19–63	ROI), NAWM		grade III 2.71 ± 0.39 %, grade IV 2.84 ± 0.30 %	II vs III P<0.001, II vs IV P<0.001, III vs IV P=0.524					fraction) had an AUC of 0.765 and 0.826, respectively. The combined use of rAPTW and IVIM parameter showed the best diagnostic performance, with an AUC of 0.986.
								rAPTW ($rAPTW = APTW_{tumor} - APTW_{CNAWM}$)	HGG 2.31 ± 0.37 % grade II 1.39 ± 0.57 % grade III 2.26 ± 0.40 % grade IV 2.37 ± 0.32 %	LGG vs HGG P<0.001, II vs III P<0.001, II vs IV P<0.001, III vs IV P=0.581	>1.71	100	84.6	LGG vs HGG 0.957	
Zhang 2018 USA Prospective	To demonstrate the value of quantitative APT for grading gliomas and detecting tumor proliferation.	APT, MT & NOE	NA	32	16 low grade 16 high grade	LGG: range, 18-66 HGG: range, 18-62	the solid portion of tumors (excluding necrosis) and whole tumors	conventional APT	the solid tumor: HGG 4.34 ± 0.95 %, LGG 4.05 ± 2.02 % whole tumor: HGG 4.46 ± 1.44 %, LGG 4.23 ± 2.06 %	P>0.05	NA	56.3	75	0.543	The fitted APT is positively correlated with Ki-67 (r = 0.451, p = 0.018). The correlation between the conventional APT and Ki-67 is not statistically significant (p > 0.05). Fitted_MT&NOE is inversely correlated with Ki-67 (r = −0.447, p = 0.019).
								fitted_APT	solid tumor: HGG 7.58 ± 0.99 %, LGG 6.79 ± 1.05 %	P =0.032	NA	75	68.8	0.723	
								fitted_MT & NOE	NA	NA	NA	81.3	68.8	0.719	
								fitted combined (direct saturation, MT&NOE, and APT)	NA	NA	NA	81.2	75	0.758	
Sakata 2018 Japan Retrospective	To examine the additive value of APT imaging alongside FDG-PET and DWI in	APT	DWI, FDG-PET	49	15 grade II 13 grade III 21 grade IV	58.3, 21–90	ROI over a slice of the tumor (enhanced area or abnormal	APT mean	LGG 0.87±0.39 % HGG 1.33±0.46 %	NA	LGG vs HGG 1.26 II and III vs IV 1.28	NA	NA	LGG vs HGG 0.76 (95%CI: 0.66–0.91) II and III vs IV 0.86 (95%CI: 0.76-0.97)	AUC (LGG vs HGG) FDG-PET 0.84, ADCmin 0.78, FDG + APTmean 0.85, ADCmin + APTmean 0.82 II+III vs IV (AUC)

Study	Aim			N	Grades	Age	ROI	Measure	LGG/HGG	P	Cutoff	Sens	Spec	AUC	Other
	grading gliomas.						signal on FLAIR)								FDG-PET 0.85, ADCmin 0.92, FDG + APTmean 0.9, ADCmin + APTmean 0.94
Togao 2017 Japan Retrospective	To investigate whether APT can differentiate HGGs from LGGs without intense contrast enhancement (CE).	APT	DWI, DSC	34	20 grade II 10 grade III 4 grade IV (only tumours without intense CE)	36.0±11.3	Whole lesion, histogram	APT 90th%tile	LGG 2.80±0.59 % HGG 3.72±0.89 %	P=0.001	2.92	85.7	70	0.811	
								APT mean	LGG 1.87±0.49 % HGG 2.70±0.58 %	P=0.0001	2.56	71.4	95	0.886	ADC mean AUC 0.593, rCBV mean AUC 0.568
Su 2017 China Prospective	To explore the utility of APT as a noninvasive biomarker of glioma proliferation and histopathologic grade by comparing APT with Ki-67 and with MRS	APT	MRS	42	1 grade I 27 grade II 6 grade III 8 grade IV	LGG: 44.00 ±2.81 HGG: 44.64 ±3.70	hot spot (4 ROI)	MTRasym mean	LGG 2.64%±0.18 HGG 3.61%±0.155	P=0.002	2.93	92.9	71.4	0.791 (95%CI: 0.650-0.931)	MTRasym (3.5ppm) values positively correlated with Ki-67 expression (r =0.502, P=.002) MTRasym (3.5ppm) values positively correlated with choline (r=0.429, P=.009) and Cho/NAA ratio (r=0.423, P =.01) and negatively correlated with NAA (r = -0.455, P=.005)
Sakata 2017 Japan Unclear	To explore relationships between MRS and APT, and to assess the diagnostic performance of MRS and APT for grading gliomas in	APT	CE T1WI, MRS	21	10 grade II 3 grade III 8 grade IV (including 2 recurrent gliomas)	50.0 ± 20.2, 11–85	VOI was placed on the area showing the solid portion of tumor on T2WI. The imaging slice in APT was set at the midpoint	APTmean	LGG 0.77±1.9 % HGG 3.2±1.4 %	NA	2.72	72.7	90	0.82 (0.62-1.00)	Positive correlations between Cho and APT90 (r=0.49), and between Cho/Cr and APTmean (r=0.65) and Cho/Cr and APT90 (r=0.59). Negative correlations between NAA/Cr and APTmean (r=-0.52). Negative correlations

Study	Objective	APT	Other	N	Grades	Age	ROI	Measure	Values	P value	Cutoff	Sens	Spec	AUC	Remarks
	comparison with CE T1WI.						of the VOI of MRS.								between NAA and APTmean (r= -0.43, P=0.05). AUC of CE 0.65, AUC of Cho 0.72, AUC of Cho/Cr 0.90
								APT90	LGG 5.0±2.8 % HGG 7.7±1.5 %	NA	6.61	90.9	70	0.77 (0.54-1.00)	
Jiang 2017_2 USA Prospective	To assess the accuracy of APT guided stereotactic biopsy to identify regions of HGG.	APT	NA	24 patients (70 specimens)	11 grade II, 6 grade III, 7 grade IV patients 33 grade II, 14 grade III, 15 grade IV, 8 edema specimens	50.5 ± 17.2	hot spot 3-6 ROI	APTmean (70 specimens)	grade II 1.82% (95% CI: 1.63-2.01) grade III 3.00% (95% CI: 2.70-3.29) grade IV 2.43% (95% CI: 1.77-3.09) edema 0.81% (95%CI: 0.47-1.15)	II vs III P < 0.001 II vs IV < 0.01	2.83	56.8	100	0.766	There was a positive correlation between APTw intensities and $Cell_{count}$ (R = 0.757; P < 0.001), and a positive correlation between APTw intensities and Ki-67 index (R = 0.538; P < 0.001).
								APTmean (the highest specimens of 24 patients)	grade II 2.07% (95% CI: 1.74-2.40) grade III 3.33% (95% CI: 3.05-3.62) grade IV 3.39% (95% CI: 2.99-3.78)	II vs III, II vs IV P<0.001	2.74	100	100	1	
Choi 2017 Korea Retrospective	To evaluate the added value of APT to ADC and rCBV in grading gliomas.	APT	ADC (DTI), DSC	46	15 grade II 10 grade III 21 grade IV	44.2 ± 14.5	hot spot (several circular ROI)	APT	grade II 0.84 ± 0.60% grade III 1.55 ± 0.87% grade IV 2.53 ±0.70% HGG 2.21 ± 0.88%	II vs IV P<0.001 III vs IV P=0.002 II vs III P=0.059	≥1.53	NA	NA	LGG vs HGG 0.877 (95%CI: 0.772–0.983)	AUC: ADC 0.888, rCBV 0.927, ADC+APT 0.910, rCBV +APT 0.923
Bai 2017 China Unclear	To evaluate grading gliomas using APT in comparison to Ki67, DWI and ASL.	APT	DWI, pCASL	44	18 grade II 10 grade III 16 grade IV	49 ± 11, 25-68	entire solid part of the tumors	APTw signal	grade II 1.25±0.17 % grade III 1.71±0.45 % grade IV 2.05±0.18 %	II vs III P=0.005 II vs IV P<0.001 III vs IV P=0.015	NA	NA	NA	II vs IV 0.997 (95% CI: 0.890-1.000) II vs III 0.825 (95%CI: 0.635-0.941) III vs IV 0.788 (95%CI: 0.584-0.921)	Correlation between APT and Ki-67 (r= 0.597). II vs IV: AUC of the ADC value 0.745, the CBF value 0.729 II vs III: AUC of the ADC value 0.767, the CBF value 0.644 III vs IV: AUC of the ADC value 0.584, the CBF value 0.481

Study	Objective	Tech1	Tech2	N	Grade	Age	ROI	Metric	Results	P-value	Col12	Col13	Col14	Col15	Col16
Togao 2016 Japan Prospective	To evaluate the dependence of saturation pulse length on APT.	APT	NA	22	9 grade II 4 grade III 9 grade IV	46.1 ± 13.8	one to five ROIs in the solid component and ROI in NAWM	MTRasym	LGG: 1.96 ± 0.69% at 0.5 s, 2.17 ± 0.50% at 1 s, 2.03 ± 0.50% at 2 s HGG: 3.09 ± 0.54% at 0.5 s, 3.83 ± 0.67% at 1 s, 4.12 ± 0.97% at 2 s	P<0.0001 for all comparisons	NA	NA	NA	NA	
								ΔMTRasym (difference between tumor and NAWM)	LGG: 0.48 ± 0.56% at 0.5 s, 1.28 ± 0.56% at 1 s, 1.88 ± 0.56% at 2 s HGG: 1.72 ± 0.54% at 0.5 s, 2.90 ± 0.49% at 1s, 3.83 ± 0.88% at 2 s	P<0.0001 for all comparisons	NA	NA	NA	NA	
Park 2016_2 Korea Retrospective	To correlate and compare diagnostic performance of APT with MRS.	APT	MRS	40	11 grade II 9 grade III 20 grade iV	LGG: 44± 16.73 HGG: 51.43±15.61	entire enhancing solid tumor or entire hyper-intense lesion on T2WI	APT90	LGG vs HGG reader1: LGG 1.1% ± 0.9, HGG 2.9% ± 1.6 reader2: LGG 1.1% ±0.9, HGG 2.9% ± 1.7	reader 1: P = 0.001 reader 2: P = 0.006	Reader 1: 1.72 reader 2 : 2.29	NA	NA	Reader 1: 0.84 (95%CI: 0.69-0.94) reader2: 0.81 (95%CI: 0.65-0.92)	MRS (Cho/Cr ratio): AUC 0.86 (95%CI: 0.71-0.95). The mean APT solid values showed a more positive correlation with the Cho/Cr ratios than with Cho/NAA ratios in both the pretreatment (r = 0.54, P < .001 vs r = 0.41, P= .011, respectively) and post-treatment groups (r = 0.43, P = .027 vs r= 0.32, P = .123, respectively).
							Standard size voxel of interest (1.5 cm³) of the solid tumor portion used for MRS	APTsolid							
Heo 2016 USA Unclear	To explore the relationship of APT and NOE with respect to different brain	APT, NOE	NA	10	6 grade II 2 grade III 2 grade IV	25, 21–65	unclear	NOE-based signals	grade II 5.18 ± 0.36% HGG 3.50 ± 0.52% grade III 3.87 ± 0.21 grade IV 3.14 ± 0.22	LGG vs HGG: P<0.05	NA	NA	NA	NA	

	tumor grades at 7T.							APT-based signals	grade II 3.08% (95%CI: 2.81% - 3.33%) grade III 2.64%(2.36% - 2.91%) grade IV 3.10% (2.85% - 3.36%)	no statistical effect	NA	NA	NA	NA
Harris 2016 USA Prospective	To present a simulation of pH weighted amine CEST contrast specific for a newly developed CEST echoplanar imaging (EPI) pulse sequence.	Amine CEST	[18] F-FDOPA PET	18	4 grade II 7 grade III 7 grade IV (mixed 12 newly diagnosed and 6 recurrent tumor)	47.6 ±15.5, 21-78	within T2 hyper-intense lesions	MTRasym at 3.0 ppm	NA	II vs III vs IV ANOVA, P = 0.0192 II vsIII, II vs IV P < 0.05 II and III vs IV P=0.0049	NA	NA	NA	NA
Sakata 2015 Japan Retrospective	To investigate the best methods of ROI and normalization for grading gliomas	APT	NA	26	8 grade II 6 grade III 12 grade IV	59.1, 21–90	whole tumor FLAIR (WT_FLAIR), whole tumour CE (WT_CE_T 1WI), single slice FLAIR (RS_FLAIR) , CE (RS_CE_ T1WI) , hot spot (4 circular ROI)s, NAWM	APT asym	WT_CE_T1WI/WT_ FLAIR/ RS_CE_T1WI/ RS_FLAIR/ MAX LGG: 0.75 ± 0.26/ 0.75 ± 0.26/ 0.78 ± 0.30/ 0.78 ± 0.30/ 1.40 ± 0.62 HGG: 1.30 ± 0.44/ 1.14 ± 0.33/ 1.35 ± 0.44/1.26 ± 0.30/ 2.23 ± 0.71	P<0.01 for all com-parisons between LGGs and HGG. P<0.01 between all com-parisons grade II and IV. P<0.05 between grade III and IV in WT_CE_	WT_CE_ T1WI/WT _FLAIR/ RS_CE_ T1WI/ RS_FLAI R/ MAX 1.11/0.89 /1.21/1.2 1/1.63	WT_CE_ T1WI/WT _FLAIR/ RS_CE_ T1WI/ RS_FLAI R/ MAX 72.2/83.3/ 77.8/72/7 7.8	WT_CE _T1WI/ WT_FL AIR/ RS_CE _T1WI/ RS_FLA IR/ MAX 100/75/ 100/100 /87.5	WT_CE_T1W I/WT_ FLAIR/ RS_CE_T1WI / RS_FLAIR/ MAX 0.85/0.83/0.8 8/0.87/0.81

										T1WI/ RS_CE_ T1WI/ RS_FLAIR.					
								Normalized APTasym (APTasym tumor - APTasym NAWM)	WT_CE_T1WI/WT_FLAIR/ RS_CE_T1WI/ RS_FLAIR/ MAX LGG: 0.54 ± 0.32/ 0.54 ± 0.32/ 0.56 ± 0.36/ 0.56 ± 0.36/ 1.19 ± 0.66 HGG: 1.10 ± 0.45/ 0.94 ± 0.33/ 1.16 ± 0.45/ 1.06 ± 0.42/ 2.03 ± 0.69	P<0.01 for all comparisons between LGGs and HGGs. P<0.01 for all comparisons grade II and IV. P<0.05 between grade III and IV in WT_CE_T1WI/ RS_CE_T1WI.	0.97/0.87/1.07/0.90/1.44	66.7/66.7/66.7/77.8/77.8	100/87.5/100/87.5/87.5	0.88/0.83/0.88/0.85/0.81	
Togao 2014 Japan Prospective	To assess the usefulness of APT in grading gliomas	APT	NA	36	8 grade II 10 grade III 18 grade IV (8 recurrent gliomas included)	48.1±14.7	hot spot (4 circular regions) in solid component (Measured APT signals in 4 ROIs averaged to represent the tumour), NAWM	mean APT	grade II 2.1±0.4% grade III 3.2±0.9% grade IV 4.1±1.0% HGG 3.8± 1.0%	grade II vs III P<0.05 grade II vs IV P<0.001 grade III vs IV P<0.05 LGG vs HGG P<0.0001	LGG vs HGG 2.54	95	100	NA	There was a moderate correlation between APT and Ki-67 (P=0.01, R=0.43). Normalized APT also correlated with Ki-67 (P<0.05, R=0.42).

								Normalized APT (tumor - NAWM)	grade II 1.8±0.7% grade III 2.9±1.6% grade IV 3.8±1.2%	gradeII vs IV P<0.01	NA	NA	NA	NA	
Zhou 2013 USA Prospective	To investigate a 3D APT imaging sequence with gradient- and spin-echo readouts (GRASE) in grading gliomas.	APT	NA	14	6 grade II 2 grade III 6 grade IV	46.5, 25–82	a single slice showing the maximum tumor area, NAWM	MTR asym	LGG 1.09% (95%CI:0.65-1.53) HGG 2.50% (95%CI:2.04-2.96)	P < 0.001	NA	NA	NA	NA	
								Tumor core - NAWM	LGG 0.51% (95%CI:0.02-1.00) HGG 2.21% (95%CI:1.68-2.74)	NA	NA	NA	NA	NA	
Zhou 2008 USA Unclear	To demonstrate a practical six-offset multi-acquisition method for APT	APT	NA	9	3 grade II 3 grade III 3 grade IV	unclear	3ROIs (tumor core, tumor periphery, and CNAWM)	APTw intensity	LGG: range, 1.0±0.3 - 1.4±0.2 HGG: range, 2.0±0.5 - 3.2±0.6	LGG vs HGG P =0.004	NA	NA	NA	NA	

Supplementary Table 3. The characteristics of the included studies for predicting molecular subtypes of gliomas

Author, year,	Main research purpose	CEST technique	Other imaging	Total N	Histology	Age (mean ± SD, range)	ROI method	Key parameter	Parameter value	P value	Cut off value	Sens	Spec	AUC	Additional results
Harris 2018 USA Unclear	To introduce a new pH- and oxygen-sensitive MRI technique using amine proton CEST echo spin-and-gradient echo (SAGE) EPI.	Amine CEST	NA	47	16 IDHmut 31 IDHwt (13 grade II, 14 grade III, 20 grade IV)	54.6 ± 16.1, 22-82	Whole FLAIR hyperintense lesion, T1WI CE (grade IV), also VOI NAWM	median MTR asym at 3.0 ppm	NA	No significant difference between IDH mutant and wild-type tumors (P=0.12); IDH mutant tumors tended to have lower R'2.	NA	NA	NA	NA	IDH mutant gliomas slightly higher degree of tumor acidity compared with IDH wild-type tumors when correcting for grade (adjusted p=0.0434)
								median R2'	NA		NA	NA	NA	NA	
Su 2018 China Retrospective	To predict MGMT protein expression in primary gliomas	APT	NA	42	38 MGMT positive 4 MGMT negative (16 grade II, 11 grade III, 15 grade IV)	MGMT positive: 44.0 ± 14.1 MGMT negative: 49.2 ± 20.1	APT visual scale 1) Not any higher signal intensity in the solid parts except cyst formations and necrosis. 2) Foggy sign, interpreted as the slightest high signal intensity with no clear borderline, like a fog. 3) Dotted or patchy hyperintensity 4) Integration of dotted and patchy hyperintensity 5) Hyperintensity on the edema and infiltrative area. The former 2 criteria were negative APTw characteristics, whereas the	true positive 36, true negative 3, false positive1, false negative 2	P=0.020	Positive vs negative	NA	NA	0.85	

						latter 3 criteria were positive APTw characteristics.							
Jiang 2018 China Retrospective	To identify MGMT promoter methlation status in GBM	APT	NA	18	8 un-methylated 10 methylated (18 GBM)	unmethylated 51.1 ± 12.4 methylated 47.3 ± 14.3 range 20-67	Enhancing lesion histogram	Mean	unmethylated 2.54±0.41 % methylated 2.01±0.42 %	0.022	2.26	87.5	80	0.825 (95%CI: 0.626–1.000)
								Variance	unmethylated 1.01±0.34 % methylated 0.59±0.24 %	0.011	0.94	62.5	90	0.837 (95%CI: 0.649–1.000)
								Skewness	unmethylated 0.04±0.52 % methylated 0.06±0.87 %	0.963	NA	NA	NA	NA
								Kurtosis	unmethylated 4.67±1.93 % methylated 4.80±3.48 %	0.934	NA	NA	NA	NA
								10th percentile	unmethylated 1.40±0.53 % methylated 1.06±0.45 %	0.186	NA	NA	NA	NA
								50th percentile	unmethylated 2.54±0.36 % methylated 1.99±0.41 %	0.012	2.25	75	80	0.850 (95%CI: 0.672–1.000)
								90th percentile	unmethylated 3.71±0.45 % methylated 2.93±0.53 %	0.006	3.25	87.5	70	0.856 (95%CI: 0.674–1.000)
								Width$_{10-90}$	unmethylated 2.31±0.42 % methylated 1.87±0.41 %	0.049	2.15	62.5	80	0.763 (95%CI: 0.537–0.988)
								Mode	unmethylated 2.45±0.38 %	0.086	NA	NA	NA	NA

Study	Aim	Index	Reference	N	Characteristics	Age	Sequence	Parameter	Values	p		Sens	Spec	AUC	Notes
									methylated 2.05±0.47 %						
Paech 2018 Germany Prospective	To investigate the non-invasive prediction of IDH mutation status, MGMT promoter methylation and differentiation of LGG and HGG.	APT, NOE	ADC, rCBV	31	8 IDHmut, 22 IDHwt MGMT 13 methylated, 9 un-methylated, 4 indeterminate 6 LGG,25 HGG	27-86, further data shown in Table1	whole onT1-GdCE, T2WI	NOE mean	IDH mut 6.03 ± 4.55 % IDH wt 9.68 ± 2.15 %	0.02	8.95	62	88	0.78	AUC: rCBV 0.79, ADC 10th% 0.72
								NOE 10th pc	IDHmut 3.63 ± 2.94 % IDHwt 4.29 ± 1.69 %	0.64	5.18	29	75	0.56	
								APT mean	IDHmut 2.30 ± 1.77 % IDHwt 4.30 ± 0.80 %	0.0032	3.66	86	86	0.88	
								APT 90th pc	IDHmut 3.36 ± 2.43 % IDHwt 6.67 ± 1.64 %	0.0019	5.22	86	86	0.9	
								dns-APT mean	IDHmut 1.10 ± 0.81 % IDHwt 2.36 ± 0.61 %	0.0011	1.88	81	100	0.92	
								dns-APT 90th pc	IDHmut 1.69 ± 1.13 % IDHwt 4.45 ± 1.53 %	0.0001	2.86	95	100	0.98	
								NOE mean	MGMT+ 7.34 ± 3.76 % MGMT- 9.97 ± 3.09 %	0.15	10.12	56	84	0.68	AUC: rCBV 90th% 0.59, ADC mean 0.59
								NOE 10th pc	MGMT+ 3.38 ± 1.88 % MGMT- 4.86 ± 2.04 %	0.13	4.6	44	77	0.69	
								APT mean	MGMT+ 3.35 ± 1.85 % MGMT- 4.34 ± 0.95 %	0.17	4.73	44	75	0.68	

								APT 90th pc	MGMT+ 5.01 ± 2.74 % MGMT- 6.18 ± 1.10 %	0.34	6.59	44	75	0.62	
								dns-APT mean	MGMT+ 1.86 ± 1.11 % MGMT- 2.35 ± 0.69 %	0.39	2.71	22	75	0.61	
								dns-APT 90th pc	MGMT+ 3.20 ± 1.93 % MGMT- 4.03 ± 1.00 %	0.34	6.59	44	75	0.62	
Jiang 2017_1 USA Retrospective	To assess the APT MRI features of IDH-wildtype and IDH-mutant grade II gliomas.	APT, MT	NA	27	7 IDHwt 20 IDHmut (27 grade II)	IDHwt 37.1 ± 7.9 IDHmut 40.5 ± 13.7	5 small ROI	maximum	IDHwt 2.03±0.72% IDHmut 0.99±0.33%	<0.001	1.67	0.57 (0.18–0.90)	1	0.89 (0.73–1)	
							6 small ROI	minimum	IDHwt 0.99±0.47% IDHmut 0.59±0.32%	0.02	1.12	0.43 (0.10–0.82)	1	0.76 (0.51–1)	
							whole	mean	IDHwt 1.39±0.49% IDHmut 0.93±0.44%	0.03	1.58	0.57 (0.20–0.94)	1	0.75 (0.52–1)	
							whole	Variance	IDHwt 0.61±0.36 % IDHmut 0.97±0.73 %	0.23	NA	NA	NA	NA	
							whole	Skewness	IDHwt -0.13±0.28 % IDHmut -0.35±0.83 %	0.5	NA	NA	NA	NA	
							whole	Kurtosis	IDHwt 0.57±0.67 % IDHmut 1.82±3.32 %	0.34	NA	NA	NA	NA	
							whole	Slope	IDHwt 2.27±0.77 %	0.33	NA	NA	NA	NA	

											IDHmut 2.65±0.91 %					
								whole	10th percentile	IDHwt 0.48±0.54% IDHmut - 0.14±0.76 %	0.06	NA	NA	NA	NA
								whole	50th percentile	IDHwt 1.39±0.46 % IDHmut 0.96±0.36 %	0.02	1.45	0.71 (0.38– 1.05)	0.95(0.85 -1.05)	0.75 (0.49 –1)
								whole	90th percentile	IDHwt 2.30±0.64 % IDHmut 1.98±0.49 %	0.18	NA	NA	NA	NA
								whole	Peak	IDHwt 1.33±0.52 % IDHmut 1.02±0.37 %	0.09	NA	NA	NA	NA
								whole	MTR mean (MT)	IDHwt 14.9±2.1 % IDHmut 16.3±5.3%	0.63	NA	NA	NA	NA

Supplementary Table 4. The characteristics of the included studies for distinction of different brain tumor types

Author, year	Main research purpose	CEST technique	Other imaging	Total N	Age (mean ±SD, range)	ROI method	Key parameter	Parameter value	P value	Cut off value	Sens (%)	Spec (%)	AUC	Additional results, comments
Yu 2017 China Unclear	To distinguish solitary brain metastasis from GBM	APT	NA	88 (43 GBM, 45 metastases)	MET 56.5 ± 9.2, 30-74 GBM 44.8 ± 13.8, 18-71	5 ROIs were distributed within enhancing tumor area	APTwmax	Tumor core MET/ GBM 2.98%± 0.74% GBM3.22%± 0.75% Peritumoral MET/ GBM 1.56%± 0.22% GBM 1.98%± 0.31%	0.141 <0.001	1.85%	93.30	69.80	0.856 (95%CI 0.764-0.921)	
							APTwmin	Tumor core MET/ GBM 2.53%± 0.70%, 2.66%± 0.63% Peritumoral MET/ GBM 0.98%± 0.25%, 1.48%± 0.34%	0.361 <0.001	1.21%	84.40	86.10	0.905 (95%CI 0.824-0.957)	
							APTwmean	Tumor core MET/ GBM 2.76%± 0.71%, 2.94%± 0.67% Peritumoral MET/ GBM 1.23%± 0.23%, 1.71%± 0.34%	0.221 <0.001	1.46%	86.70	81.40	0.868 (95%CI 0.779-0.931)	
							rAPTwmax	Tumor core MET/ GBM 2.51%± 0.79%, 2.67%± 0.73% Peritumoral MET/ GBM 1.09%± 0.22%, 1.43%± 0.31%	0.305 <0.001	1.27%	80.00	76.70	0.829 (95%CI 0.734-0.901)	
							rAPTwmin	Tumor core MET/ GBM 2.03%± 0.71% 2.10%± 0.58% Peritumoral MET/ GBM 0.51%± 0.29% 0.95%± 0.30%	0.578 <0.001	0.71%	77.80	85.50	0.864 (95%CI 0.774-0.927)	
							rAPTwmean	Tumor core MET/ GBM 2.28%± 0.76%, 2.40%± 0.65% Peritumoral MET/ GBM 0.76%± 0.27%, 1.17%± 0.32%	0.448 <0.001	1.09%	82.20	74.40	0.841 (95%CI 0.748-0.911)	
Shen 2017 China Prospective	To compare NOE signals between glioma and meningioma	APT, NOE	NA	11 (6 gliomas grade unclear, 5 meningioma)	48.1 ± 13.9	A gadolinium contrast enhanced region	MTR asym at 3.5 ppm, NOE*%	NA	NA	NA	NA	NA	NA	Difference between tumor and CNAWM in NOE*% at −3.5 ppm for glioma (p < 0.001).
Khlebnikov 2017	To provide insight into the effect of water	APT, 3 metrics	NA	6 (2 grade II and 3 grade IV	49±13.4	NAWM (ROI 1), edema (ROI 2),	MTR Rex AREX MTRasym	NA	NA	NA	NA	NA	NA	Distinction between low and high-

Netherlands Unclear	T1 relaxation on APT			gliomas, 1 meningioma)		normally appearing gray matter (NAGM, ROI 3), Gadolinium-enhanced tumor (ROI 4), non-enhanced solid tumor (ROI 5), and non-enhanced cysts (ROI 6)								grade gliomas based on Gd non-enhanced solid tumor regions in MTR Rex; but this difference becomes negligible after T1w is accounted for in AREX.
Jeong 2017 Korea Retrospective	To characterize APT signals in acute and subacute haemorrhage brain lesions	APT	NA	23 (16 tumor (3 GBM, 9 metastases, 2 pituitary adenoma, 1 hemangio-blastoma, 1 angio-sarcoma, and 7 non-tumor)	52.7 ± 12.8	Within the enhancing portion, in haem-orrhage and in normal-appearing white matter	MTRasym	Acute haemorrhage/subacute/ enhancing portion/NAWM Tumor: 3.69 ± 1.52 %/ 1.44 ± 0.84 %*/ 2.65 ± 0.92 %*/0.24 ± 0.59 %* Non-tumor: 3.67 ± 0.54 %/ 1.83 ± 0.82 %*/NA/0.71 ± 0.39 %*	Tumor vs non-tumor 0.967/0.774/NA/ 0.317 *MTRasym values that are different from those of acute haemorrhage in each group (P value < 0.05).	NA	NA	NA	NA	
Jiang 2016 China Retrospective	To differentiate PCNSLs from HGGs	APT	NA	32 gliomas (21 HGG, 6 grade II, 15 grade IV)	PCNSL 55.3±13.7, 36−79 HGG 45.0±14.6, 22−66	5 ROIs in enhancing lesion	APTWmax	PCNSL3.38%±1.06% HGG 4.36 %±1.30 %	P<0.05	3.13%	95.20%	53.80%	0.707 (95%CI 0.518–0.896)	
							APTWmin	PCNSL 2.62 %±0.90 % HGG 1.81 %±0.65 %	P<0.01	2.47%	85.70%	61.50%	0.751 (95%CI	

							Metric	Results	P-value	Cutoff	Sens	Spec	AUC	Notes
													0.566–0.936)	
							APTWmax-min	PCNSL 0.76%±0.42% HGG 2.55 %±1.20 %	P<0.01	1.14%	100%	84.60%	0.963 (95%CI 0.901–1.000)	
							CESTtotal	PCNSL 11.22 %±3.47 % HGG 14.34 %±4.04 %	P<0.05	10.69%	95.20%	53.80%	0.733 (95%CI 0.555–0.910)	
							MTR	PCNSL 19.22 %±3.36 % HGG 13.43 %± 5.40 %	P<0.01	15.60%	61.90%	92.30%	0.828 (95%CI 0.687–0.969)	
							APTWmean	PCNSLs (3.01%±0.98%) HGGs (3.06 %±0.81 %, P=0.879)	P=0.879	NA	NA	NA	NA	
Park 2015 Korea Retrospective	To determine whether APT provides increased accuracy of DSC	APT	DSC	45 contrast enhanced tumors (6 grade I 4 pilocytic astrocytoma, 2 hemangio-blastoma), gliomas 13 grade II (including 3 PXA), 10 grade III, 11 grade IV, 5 metastasis	Male: mean age, 42.2 years; range, 29–75 years. Female: mean age, 45.7 years; range, 27–61 years	Entire solid portion, histgram	APT90	Low grade tumors 2.1 ± 0.9% for reader 1 and 2.3 ± 0.8% for reader 2 High grade tumors 4.1 ± 1.3% for reader 1 and 4.0 ± 1.2% for reader 2	P<0.01	3.5% for reader 1 3.7% for reader 2	NA	NA	0.85 (95%CI 0.74-0.92) for reader 1 0.86 (95%CI 0.75-0.94) for reader 2	Adding APT90 improved tAUC for identification of contrast-enhancing low-grade tumor from 0.80 to 0.97 for reader 1 (P = .023) and from 0.82 to 0.97 for reader 2 (P= .035)
Jones 2006 USA Unclear	To quantify the APT effect at 3T in patients with brain tumors.	APT	NA	10 gliomas (5 grade II, 1 grade III, 2 grade IV)	Unclear	Hotspot, whole lesion	APT hotspot	Data for 7 tumours: Grade II 5.5±0.3 %, 1.9 ±0.07 %, 1.9±0.06 %, -0.2 ±0.05 % GBM 1.9 ± 0.06 %, 4.1 ± 0.2 % meningioma 3.5 ± 0.09 %	NA	NA	NA	NA	NA	

Supplementary Table 5. The characteristics of the included studies for differentiating tumor recurrence from treatment-related changes

Author, year	Main research purpose	CEST tech-nique	Other imaging	Total N	Therapy	Histology	Imaging follow up or tissue diagnosis	Age (mean ± SD, range)	ROI method	Key param eter	Parameter value	P value	Cut off value	Sens %	Spec%	AUC	Additional results
Park 2018 Korea Retro-spective	To compare the diagnostic per-formance of APT and MET-PET	APT	11C MET-PET	43	Tumor resection or stereotactic biopsy, radiation or concurrent chemoradiation according to standard protocol	12 grade II, 4 grade III, 27 grade IV 38 recurrence (12 LGG, 26 HGG), 5 treatment related change (HGG)	31 second-look operation, 12 non-surgical follow up using RANO criteria	52.1, 32–73	100-mmcircular ROIs of highest value (APT max), entire solid en-hancing lesion (90% histgram cut-off: APT90)	APT max	LGG 1.94 % (interquartile range; 0.49–2.73) HGG 3.00 % (interquartile range; 2.29–4.04)	0.02	2.03%	86.2	85.7	Post-treatm ent HGGs 0.88 (95%CI : 0.72-0.96)	MET-PET: TNRmax AUC 0.71, TNR 90 AUC reader 1 0.53, reader 2 0.59
										APT90	Reader 1 LGG 1.09 % (interquartile range; -0.31–1.64) HGG 2.60 % (interquartile range; 1.18–3.58) reader2 LGG 1.15 % (interquartile range; 0.0–1.99) HGG 2.62 % (interquartile range; 1.69–3.64)	Reader 1 = 0.01, reader 2 = 0.034	1.79% 1.96%	85.7 80.1	80.0 89.7	Post-treatm ent HGGs 0.83 (95%CI : 0.66 - 0.94) 0.78 (95%CI : 0.60 - 0.91)	
Mehrabian 2017 Canada Prospective	To differentiate radiation necrosis and tumour progression	APT, MT, NOE	NA	16	Stereotactic radiosurgery (SRS) and chemotherapy	Metastasis 5 progression, 11 radiation necrosis	9 patients surgical resection, 7 patients non-surgical managment.	39-73	ROI covering en-hancing tumour (incl.	NOEM TR (%)	Necrosis 8.9 ± 0.9 %, PD 12.6 ± 1.6 %	<0.000 1	NA	NA	NA	NA	
										Amide MTR (%)	Necrosis 8.2 ± 1.0 %, PD 12.0 ±1.9 %	<0.000 1	NA	NA	NA	NA	

Study	Aim			N	Treatment	Outcome				Metric	Value	p				AUC	Conclusion
							(central necrosis)			MT (%)	Necrosis 4.7 ± 1.0 %, PD 6.7±1.7 %	0.009	NA	NA	NA	NA	
										NOEAUC (% Hz)	Necrosis 4.3 ± 2.0 % Progression 7.2±1.9 %	0.019	NA	NA	NA	NA	
										Amide AUC (% Hz)	Necrosis 2.0 ± 1.3 %, PD 3.0±2.2 %	0.23	NA	NA	NA	NA	
										APT (%)	Necrosis ⁻0.7 ± 1.0 %, PD -0.6±1.0 %	0.89	NA	NA	NA	NA	
Park 2016_2 Korea Retrospective	To compare diagnostic performance of APT with MRS	APT	MRS	21 treated	Resection >75% followed by either radiation therapy or concurrent chemotherapy and radiation therapy	13 tumor progression (TP), 8 treatment related effect (TE) 4 grade III, 17 grade IV		PD: 54 ± 12.22, Treatment Effects: 50.33 ± 14.60	Entire T1WI-CE solid tumour or entire lesion on T2WI	APT90	Reader 1: TP 2.7± 0.8 %, TE 0.9 ± 0.8 % Reader 2: TP 2.8± 1.4 %, TE 0.8± 0.9 %	0.021	reader 1: 1.90 reader 2: 1.98	NA	NA	0.90 (95%CI 0.70-0.99) 0.89 (95%CI 0.69-0.99)	APT accuracy is 72% for Reader 1 and 72% for Reader 2.
Park 2016_1 Korea Retrospective	To determine the added value of APT to conventional and perfusion MRI	APT	Conventional, DSC	65	CCRT after surgical resection not exposed to other chemotherapeutic agents, including bevacizumab	37 tumor progression (TP), 28 treatment related effect (TE) GBM	RANOcriteria 14 second look surgery, 51 follow up	54.3; 24–77	Entire T1WI-CE lesion	APT90 Expert	TP 3.87±1.72 % TE 1.38±1.14 %	<0.001	2.88	NA	NA	0.89	CE-T1WI APT90: AUC 0.91 CE-T1WI (SWE + SE) + APT90 + nCBV90: AUC 0.97
										APT90 trainee	TP 4.01±1.87 % TE 1.41±1.07 %	<0.001	2.52	NA	NA	0.89	CE-T1WI APT90: AUC 0.90 CE-T1WI (SWE + SE) + APT90 + nCBV90: AUC 0.96

Ma 2016 USA Unclear	To distinguish true progression from pseudo-progression	APT	NA	32	Chemoradiation	20 true progression (2 grade II, 5 grade III, 13 grade IV), 12 pseudo-progression (1 grade II, 2 grade III, 9 grade IV)	RANO criteria	56.5, 22-78	3-5 ROI	APTW mean	True 2.75% 0.42% pseudo 1.56% 0.42%	<.001	2.42	85	100	0.98	
										APTW max	True 3.29% 0.61% pseudo 1.95% 0.44%	<.001	2.54	95	91.7	0.97	

Supplementary Table 6. The characteristics of the included studies for therapy response assessment and prognosis prediction

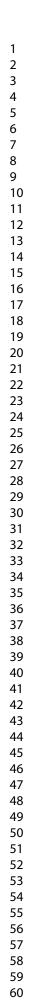| Author year	Main research purpose	CEST tech-nique	Other imaging	Total N	Histology	Age (mean ± SD, range)	Therapy	Reponse assessment	ROI method	Key parameter	Para-meter value SD	Para-meter value PD	P value	AUC	Sens	Spec	Other results
Regnery 2018 Germany Prospective	To investi-gate CEST in GBM as predictor of early tumor progression after first-line treatment	NOE, APT	T2WI, ADC	20	Grade IV GBM 12 stable disease, 8 early progression	Median 60 (inter-quartile range 53-69)	Resection in 12 patients, no resection in 8. All underwent adjuvant radiotherapy (60 Gray, 30 fractions) with con-comitant (75 mg/m²) and adjuvant (150–200 mg/m²) TMZ. Radiothera py adapted in 5 elderly patients.	Based on clinical 3T MRI and neurological evaluation derived at 1st and 2nd follow-up examinations (approx. 1 and 3 months post radiotherapy). Following the updated RANO criteria.	Manual segment-ation of whole tumor region including all areas of abnormal signal intensity on T1WI-CE and T2WI images	NOE-LD	11.66 (interquar tile range 11.18–12.31)	10.37 (10.31 – 10.48)	0.0001	0.98 (95%CI 0.92 – 1.00)	0.91	1	
										NOE-AREX	9.91(9.25 – 11.90)	8.95 (8.25 – 9.87)	0.1288	0.72 (0.48 – 0.95)	0.64	0.75	
										NOE weighted MTRasym	−5.71 (−6.41 – 4.82)	-4.52 (−4.90 – 3.39)	0.0186	0.83 (0.64 – 1.00)	0.73	1	
										APT-LD	5.28(5.12 – 5.39)	5.36 (4.90 – 6.06)	1	0.50 (0.18 – 0.82)	0.91	0.38	
										APT-AREX	4.22 (3.85 – 4.76)	4.73 (4.27 – 4.80)	0.3421	0.64 (0.37 – 0.90)	0.64	0.75	
										dns (downfield NOE supressed) APT	2.14 (1.92 – 2.28)	2.71 (2.56 – 3.09)	0.0328	0.80 (0.57 – 1.00)	0.82	0.88	
Desmond 2017 Canada Unclear	To determine the predictive value of CEST metrics in brain metastases treated with stereotactic	APT, NOE, MT, amine	NA	25 pre-therapy 17 follow up at 1 week 20 one-month volume	Brain metastases (Majority with primary tumors in lung and breast, also rectal cancer and melanoma)	62±14	All patients received SRS, in which a single dose of 18 to 20 Gy of radiation	Volume of tumor (1) pretreatment baseline (up to 1 week before therapy); (2) 5 to 8 days post-therapy (the 1-week	ROIs in enhancing tumor, edema, necrotic core, NAWM	APTw	NA	NA	NA	NA			1 week predictive value No correlation was observed between changes in APTw at 1 week and volume changes in any of the ROIs. baseline predictive value No significant correlation (P>=0.05) was observed between volume changes and APTw at baseline. For all metrics at both the baseline and 1-week predictive time points, the correlation with therapy response

											Metric					Results
	radio-surgery (SRS)								time point); and (3) 1 month post-therapy. All had a pre-treatment data set, 5 had neither of the follow-up scans, 5 were missing the final time point, and 1 was missing 1-week post-treatment data, but had the 1-month post-treatment time point. One of the patients missing CEST at the final time point still had tumor volume measured, and 2 had tumors that were not visible on CEST MRI.		Peak fit metrics	NA	NA	NA	NA	was greater with ROIs in the NAWM and edema than within the enhancing tumor.
																1 week predictive value. Significant correlation was observed between volume changes and the relative change in NOE peak amplitude in contralateral NAWM (R=0.69; P=0.0021;n=17), in ipsilateral NAWM (R=0.56; P=0.019; n=17), and in MT peak amplitude in edema (R=0.77; P=0.027; n=8). Baseline predictive value. For the peakfit metrics, a significant correlation (P<0.05) was observed between volume changes and NOE amplitude in contralateral NAWM (R=–0.69; P=0.0022; n=17).
											AREX metrics	NA	NA	NA	NA	1 week predictive value. The change in AREX metric calculated at the NOE offset frequency in the contralateral NAWM was also positively correlated with tumor volume changes (R=0.59; P=0.033; n=13). Within the tumor, there was a significant negative correlation between the volume changes at 1 month and the absolute change in the NOE width (R=-0.55; P=0.028; n=18), as well as the absolute change in amine AREX (R=0.58; P=0.039; n=13). Baseline predictive value. The baseline NOE AREX in contralateral NAWM was also significantly correlated (R=–0.65; P=0.011; n=14)
Harris 2015 USA	To examine differences in PFS	Amine CEST	18 FDOPA PET,	25 (3 gliomas			Maximal surgical resection	Evaluated at 3 time points—(i)	not place ROI	MTRasym at 3.0ppm	NA	NA	NA	NA	Patients with tumors that were acidic at baseline , defined by a significant region (>50%) of positive CEST

Prospective			DTI, MRS, DSC	(WHOIII-IV) pH weighted MRI, F-FDOPA PET, and MRS, 2 gliomas WHO II and IV) for pH weighted MRI-guided biopsy, and 20 newly diagnosed GBM			followed by standard treatment with radiotherapy and concurrent temozolomide	baseline: postsurgical and prior to radiochemotherapy; (ii) midtreatment: ~3weeks after the start of radiochemotherapy; and (iii) posttreatment: ~6–10 weeks after the start of radiochemotherapy, or 0–4 weeks after completion of concurrent radiation and chemotherapy. s determined by RANO criteria		asymmetry at 3.0 ppm within areas of contrast enhancement and/or T2 or FLAIR hyperintensity, demonstrated a significantly longer PFS compared with patients lacking significantly acidic tumors (log-rank, P<.0001; median PFS for acidic tumors vs non-acidic tumors=125 days vs 450 days). Patients exhibiting an increase in the size of acidic lesions during concurrent radiation and temozolomide had a significantly shorter PFS from the end of radiation therapy compared with tumors exhibiting stable or decreasing acidic lesion size (log-rank, P=.0003; median PFS in acidic grow-ing tumors=68 days vs 339 days),

1
2
3
4
5
6
7
8
9
10
11
12
13
14
15
16
17
18
19
20
21
22
23
24
25
26
27
28
29
30
31
32
33
34
35
36
37
38
39
40
41
42
43
44
45
46
47
48
49
50
51
52
53
54
55
56
57
58
59
60

Studies identified by database search (n = 430)
   174 from PubMed
   240 from Cochrane Library
   16 from Embase

323 studies after duplicates removed

Studies excluded on title/abstract (n = 255)

Full-text studies assessed for the meta-analysis (n = 68)

Studies excluded (n = 32)

  3 animal studies
  21 not examine diagnostic or prognostic value
  4 less than 5 patients
  4 review

Studies included in systematic review (n = 36)

  - grading gliomas (n = 19)
  - predicting molecular subtypes (n = 5)
  - diagnosing different type of brain tumors (n = 7)
  - differentiating recurrence from treatment-related changes (n = 5)
  - therapy response assessment (n = 3)

Figure 1. Flow chart describing the study selection process. Two studies contained data on glioma grading and predicting molecular subtypes, and one study was assigned to both glioma grading and differentiating recurrence from treatment-related changes.
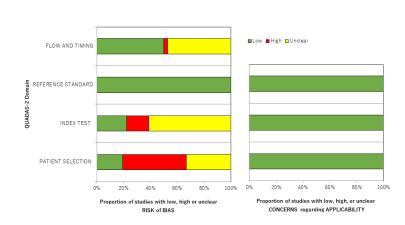
210x289mm (96 x 96 DPI)

Figure 2. Results of the QUADAS2 quality assessment of the included studies. The risk of bias in four different domains and concerns regarding applicability in three domains are shown.

338x190mm (96 x 96 DPI)